minerals

MDPI

Article

Mineralogy of Phoscorites of the Arbarastakh Complex (Republic of Sakha, Yakutia, Russia)

Mikhail Nikolaevich Kruk [1,*], Anna Gennadievna Doroshkevich [1,2], Ilya Romanovich Prokopyev [1,3] and Ivan Aleksandrovich Izbrodin [1,2]

1 Sobolev Institute of Geology and Mineralogy, Siberian Branch of the Russian Academy of Sciences, 630090 Novosibirsk, Russia; doroshkevich@igm.nsc.ru (A.G.D.); prokopev_ilya@mail.ru (I.R.P.); isbrodin@rambler.ru (I.A.I.)
2 Geological Institute, Siberian Branch of the Russian Academy of Sciences, 670047 Ulan-Ude, Russia
3 Department of Geology and Geophysics, Novosibirsk State University, 630090 Novosibirsk, Russia
* Correspondence: krukmn@igm.nsc.ru; Tel.: +7-913-981-40-34

Abstract: The Arbarastakh ultramafic carbonatite complex is located in the southwestern part of the Siberian Craton and contains ore-bearing carbonatites and phoscorites with Zr-Nb-REE mineralization. Based on the modal composition, textural features, and chemical compositions of minerals, the phoscorites from Arbarastakh can be subdivided into two groups: FOS 1 and FOS 2. FOS 1 contains the primary minerals olivine, magnetite with isomorphic Ti impurities, phlogopite replaced by tetraferriphlogopite along the rims, and apatite poorly enriched in REE. Baddeleyite predominates among the accessory minerals in FOS 1. Zirconolite enriched with REE and Nb and pyrochlore are found in smaller quantities. FOS 2 has a similar mineral composition but contains much less olivine, magnetite is enriched in Mg, and the phlogopite is enriched in Ba and Al. Of the accessory minerals, pyrochlore predominates and is enriched in Ta, Th, and U; baddeleyite is subordinate and enriched in Nb. Chemical and textural differences suggest that the phoscorites were formed by the sequential introduction of different portions of the melt. The melt that formed the FOS 1 was enriched in Zr and REE relative to the FOS 2 melt; the melt that formed the FOS 2 was enriched in Al, Ba, Nb, Ta, Th, U, and, to a lesser extent, Sr.

Keywords: phoscorites; Arbarastakh alkaline-ultrabasic carbonatite complex complex; mineralogy; chemical evolution; Aldan shield

check for updates

Citation: Kruk, M.N.; Doroshkevich, A.G.; Prokopyev, I.R.; Izbrodin, I.A. Mineralogy of Phoscorites of the Arbarastakh Complex (Republic of Sakha, Yakutia, Russia). *Minerals* **2021**, *11*, 556. https://doi.org/10.3390/min11060556

Academic Editors: Anna A. Nosova and Alexey V. Kargin

Received: 12 April 2021
Accepted: 18 May 2021
Published: 24 May 2021

Publisher's Note: MDPI stays neutral with regard to jurisdictional claims in published maps and institutional affiliations.

Copyright: © 2021 by the authors. Licensee MDPI, Basel, Switzerland. This article is an open access article distributed under the terms and conditions of the Creative Commons Attribution (CC BY) license (https://creativecommons.org/licenses/by/4.0/).

1. Introduction

Alkaline carbonatite complexes are composed of a unique group of igneous rocks that contain information about the deep processes of the mantle, which determine the composition of alkaline silicate and carbonatite melts. Carbonatites can be formed by direct melting of the carbonatized mantle peridodite [1–3] during the process of fractional crystallization of CO_2 saturated silicate magmas [4] or as a result of carbonate–silicate liquid immiscibility [5,6]. Deposits of highly charged elements (Nb, Ta, Ti, Zr), REE, radioactive elements (Th and U), iron, copper, apatite, fluorite, and others are associated with alkaline carbonatite complexes [7–14].

Some carbonatites are spatially related to phoscorites, which are defined as carbonate-bearing ultrabasic rocks consisting of magnetite, apatite, forsterite, diopside, or phlogopite [15]. A total of 21 phoscorite occurrences have been described, which are located around or in carbonatite cores—for example, Palabora Carbonatite Complex [13] and Kovdor Complex [7]. The spatial relationship of carbonatites and phoscorites determines their genetic relationship, and to date, several mechanisms for the origin of phoscorites have been proposed: the metasomatic model, crystallization from a melt of phoscorite composition; fractional crystallization or liquation from a carbonatite melt [7,13,15–18].

The metasomatic model has not found an application due to the numerous geological, petrological, and mineralogical data obtained and the results from studying inclusions, which confirm the formation of early carbonatites and phoscorites from a magmatic melt. However, the available experimental data do not make it possible to establish whether phoscorites were formed due to fractional crystallization or liquid immiscibility [19].

The processes of carbonate–silicate immiscibility are involved in the formation of ore-bearing carbonatite complexes with Nb, Zr, and REE mineralization [20,21]. However, recent experimental data show that the distribution coefficients of Nb, Ta, Hf, and Zr between carbonate and silicate melts are less than 1, and, therefore, these elements cannot be more concentrated in a carbonate melt that has separated immiscibly from a silicate melt [22].

The Arbarastakh alkaline-ultrabasic carbonatite complex (Russia) is a typical example of an association of alkaline silicate rocks with carbonatites and phoscorites located in the central part of the complex. Modern information on the rocks of the Arbarastakh complex is very limited. The available geochronological data show that the crystallization ages yield 690 ± 28 Ma for the carbonatites and 720 ± 28 Ma for the phoscorites (K–Ar, phlogopite) [23]. The age of the rocks corresponds to the Neoproterozoic stage of alkaline carbonatite magmatism (725–630 Ma) in the southern part of the Siberian Craton, including the formation of ore-bearing alkaline-ultrabasic carbonatite complexes, such as Belaya Zima, Middle Zima, Tagna, Zhida, Ingili, Gornoe Ozero [24]. The results of the melt inclusions studies in minerals from the carbonatites and phoscorites of Arbarastakh indicate that the carbonatites were formed from an alkaline silicocarbonatite melt, while the phoscorites are the products of the differentiation of the carbonatitic melt [25].

New data on petrography, mineralogy, and the compositional trends of minerals from the the Arbarastakh complex phoscorites are presented in this article. Based on the data obtained, the genetic aspects of the formation of phoscorites are discussed.

2. Geological Setting

The Arbarastakh ultramafic alkaline carbonatite complex is located in the Republic of Sakha (Yakutia) in southeastern Russia, in the Arbarastakh River basin, a left tributary of the Idyum River (Lena River basin). The complex is located in the eastern part of the Aldan–Stanovoy shield, which is part of the Siberian Craton (Figure 1a). Smelov and Zedgenizov [26] distinguish five terranes within the Aldan–Stanovoy shield (West Aldan, Central Aldan, East Aldan, Tyndinsky, and Chogarsky) separated by zones of tectonic melange (Amginsky, Kalarsky, and Tyrkandinsky) (Figure 1a). The Arbarastakh complex is located on the Uchur granulite–paragneiss terrane, which is composed mainly of Archean hornblende, biotite, diopside, hypersthene crystalline schists, gneisses, amphibolites, garnet gneisses, marbles, and calcareous silicate rocks [26].

The Arbarastakh complex has a concentric zonal structure. According to Glagolev et al. [23], the main phases composing the complex are pyroxenites, currently classified as jacupirangites—biotite-bearing mela-ijolite [25]. Numerous bodies of silicocarbonatites, calcite carbonatites, phoscorites, and alkali-feldspar syenites have cleavesplit contacts with the main phases. The complex also contains dikes of ultrabasic lamprophyres [25]. The host rocks are represented by Archean granites and metamorphic rocks, which form a series of isoclinal folds steeply dipping towards to the northeast [23]. The base of the complex is a stock-like body of the jacupirangites elongated in the northwestern direction (Figure 1b). Between the body of the jacupirangites and the host rocks, there is a fenite zone up to 1 km thick. The phoscorites, carbonatites, and silicocarbonatites of the Arbarastakh complex are concentrated within the jacupirangite body and are represented by dike-like bodies (Figure 1b). The dikes have a thickness of 10–20 cm to 400 m and cleave contacts with jacupirangites. The incidence angles do not change depending on their position in the massif and are 60–80° [23]. It should be noted that the phoscorites cut the silicocarbonatites [23]. Dikes of ultrabasic lamprophyres are located in the central part of the complex and have thicknesses of 0.1 to 1 m. Feldspar syenite dikes are localized in the endocontact zone of the complex and have cleave contacts with jacupirangites

and fenites (Figure 1b). A geological study of the complex showed the following geological sequence of rock formation: jacupirangites → carbonatites and phoscorites → dikes of feldspar syenites [25].

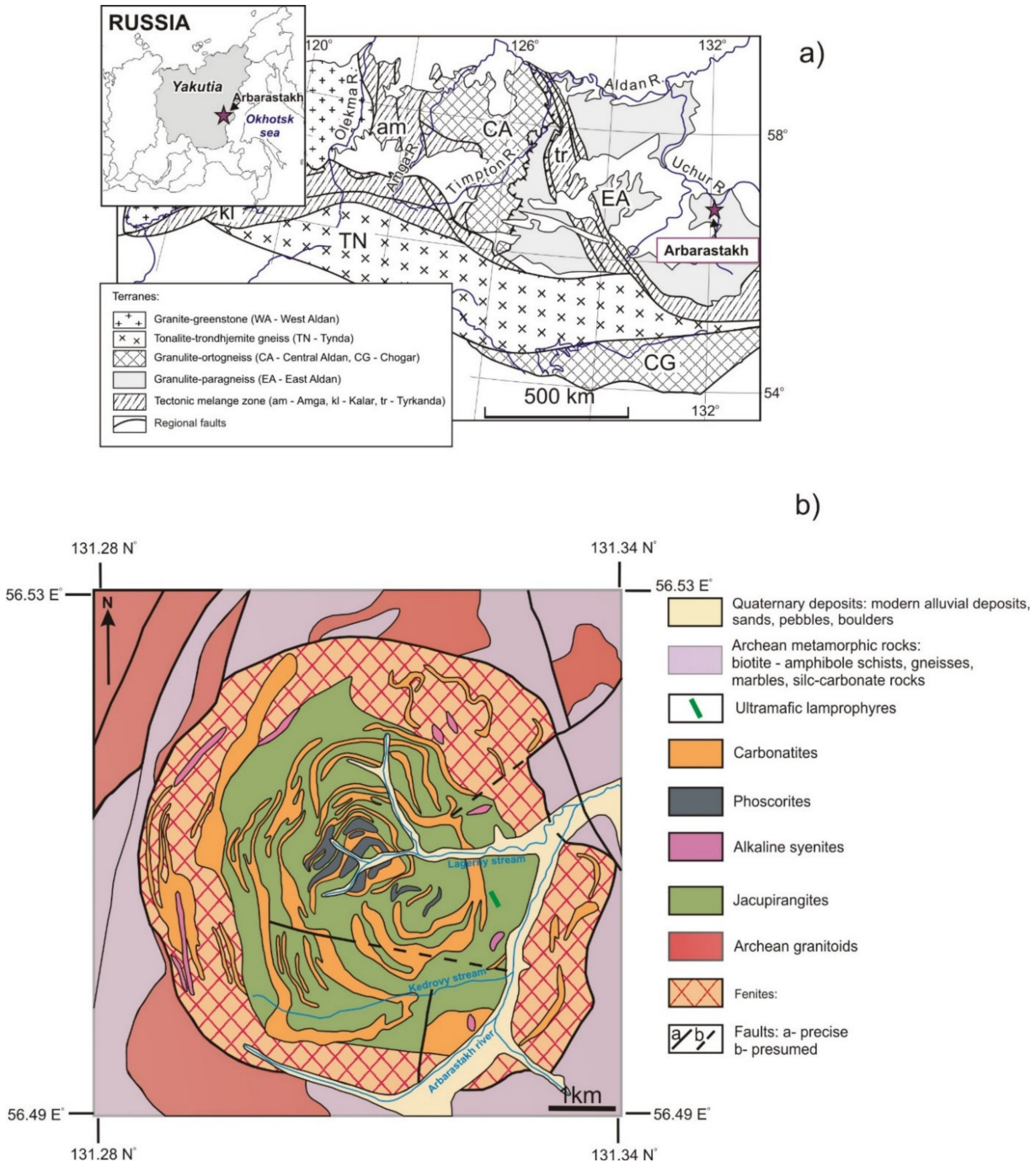


Figure 1. (**a**) Location of the ultramafic alkaline carbonatite complex Arbarastakh in Yakutia (Republic of Sakha), southeast of Russia (upper left inset) within the Aldan-Stanovoy shield (modified after [26]). (**b**) Scheme of the geological structure of the complex [23].

3. Analytical Methods

The polished sections of each sample were examined by transmitted and reflected light microscopy under a polarizing microscope (Olympus, Tokyo, Japan) equipped with a camera. The polished rock samples were used to determine the rock textures and min-

eral assemblage compositions using energy-dispersive spectrometry in combination with back-scattered electron imaging (BSE) using a TESCAN MIRA 3 LMU JSM-6510LV (manufactured by Tescan, Brno, Czech Republic) scanning electron microscope (SEM) with the energy module from X-Max Oxford Instruments for microprobe analysis. Mineral composition was determined using a JEOL JXA-8100 (Jeol, Tokyo, Japan) electron microprobe (WDS mode, 20 kV, 15 nA, beam diameter 1–2 μm). For calibration, both natural minerals and synthetic phases were used as standards.

The peak counting time was 15–20 s (10 s for peak counting and 5–10 s for background counting). The studies were carried out at the Analytical Center for Multielement and Isotope Research of the Siberian Branch of the Russian Academy of Sciences (Novosibirsk, Russia). The analytical conditions and the set of standards are described in Electronic Supplement 1 (Supplementary Materials).

The structural formulae of magnetite are normalized to three cations. The structural formulae of apatite were calculated for eight cations. For different trends of substitution in apatite for the structural formula $A_5(ZO_4)_3(Y)$, the following preferable fillings of positions with elements are assumed: position A: Na^+–Ca^{2+}–Sr^{2+}–Fe^{2+}–Mn^{2+}–Ba^{2+}–REE^{3+}; position Z: Si^{4+}–P^{5+}–S^{6+}; position; Y: F^-–Cl^-–$(OH)^-$. OH was calculated assuming (F + Cl + OH) = 1.

The structural formulae of micas were calculated based on the formula (AB_3 $[Z_4O_{10}]$ $[Y]_2$), and the data were normalized to seven cations (Z + B) [27]. Earlier studies have shown that calculations of Fe^{2+}/Fe^{3+} from microprobe analysis are reliable when appropriate recalculation methods are used [28]. For different trends of substitution in phlogopite, the following cations occupy the following positions: position A: K^+–Na^+–Ca^{2+}–Sr^{2+}-Ba^{2+}; position B: Mg^{2+}–Fe^{2+}–Mn^{2+}–Al^{3+}–Ti^{4+}; position Z: Si^{4+}–Al^{3+}–Fe^{3+}; position; Y: F^-–Cl^-–$(OH)^-$. OH was calculated assuming (F + Cl + OH) = 2.

The structural formulae of baddeleyite were calculated for two oxygens. The structural formulae of zirconolite were calculated for 28 charges. With different trends of substitution in zirconolite, the following cations occupy the following positions (assuming the structural formula as $A_2B_2C_4O_{14}$): position A: Ca^{2+}–Mg^{2+}–Fe^{2+}–Mn^{2+}–Ba^{2+}–REE^{3+}; position B: Zr^{4+}–Hf^{4+}–U^{3+}–Th^{3+}; position C: Si^{4+}–Ti^{4+}; Fe^{2+}–Nb^{5+}–Ta^{5+}.

The structural formulae of pyrochlore were calculated based on the formula $A_2B_2(O,OH)_6Y$ and normalized to two cations in position B [29]. For different trends of substitution in pyrochlore, the following cations occupy the following positions: position A: Mg^{2+}–Ca^{2+}–Ba^{2+}–Na^+–K^+–U^{4+}–Th^{4+}–REE^{3+}–Sr^{2+}–Pb^{2+}; position B: Nb^{5+}–Ta^{5+}–Ti^{4+}–Zr^{4+}–Si^{4+}–Al^{3+}–Fe^{2+}; position Y: F^-–$(OH)^-$.

The investigations were carried out at the Analytical Center for Multi-Elemental and Isotope Research Siberian Branch, Russian Academy of Science (Novosibirsk, Russia). A complete set of microprobe analyzes as well and the calculation of the apfu. can be found in Table S1 (Supplementary Materials).

4. Results of Investigations

4.1. Decription of Arbarastakh Phoscorites

According to the mineral composition, the spatial ratio of the minerals, and the structural and textural characteristics, the phoscorites are conditionally divided into two groups: baddeleyite-containing (FOS 1) (Figure 2a) and pyrochlore-containing (FOS 2) (Figure 2b). The FOS 1 phoscorites are fine-to-medium-grained, with rare phenocrysts of magnetite, and consist mainly of apatite (35–40%), olivine (25–30%), magnetite (20–25%), and a significant amount of phlogopite (5–15%). Minor and accessory minerals are baddeleyite (up to 1%), ilmenite, sulfides such as pyrite and chalcopyrite (up to 1%), as well as pyrochlore and zirconolite. Olivine is present as sub-idiomorphic grains up to 4 mm in size. Apatite forms two textural varieties: the first form sub-idiomorphic grains with rounded edges up to 5 mm length with rare inclusions of phlogopite or idiomorphic grains no larger than 1 mm found in the form of inclusions in magnetite and baddeleyite. The second form of apatite often contains inclusions of phlogopite, zirconolite, and pyrochlore. Phlogopite also forms

two textural varieties—the first variety forms medium (up to 3 mm) sub-idiomorphic brown plates with pronounced pleochroism, the edges of the grains are darker in color; the second variety forms idiomorphic grains—which appear as inclusions in magnetite and apatite (Figure 3a). Magnetite forms grains of irregular shape, which can vary greatly in size: from millimeters to 2–3 cm. Magnetite grains often contain various inclusions of phlogopite, apatite, pyrochlore, and zirconolite. Sulfides are found throughout the rock. The baddeleyite in FOS 1 forms large (up to 2 mm) idiomorphic homogeneous grains, often corroded, in which inclusions of apatite are found (Figure 3c). Pyrochlore and zirconolite form idiomorphic grains up to 50 mcm in size, occurring as inclusions in apatite, less often in magnetite. The grains of these minerals can be either homogeneous or zonal (Figure 3d). Ilmenite is rarely present in the form of inclusions in magnetite grains but forms sub-idiomorphic grains of up to 30–40 mcm in diameter.

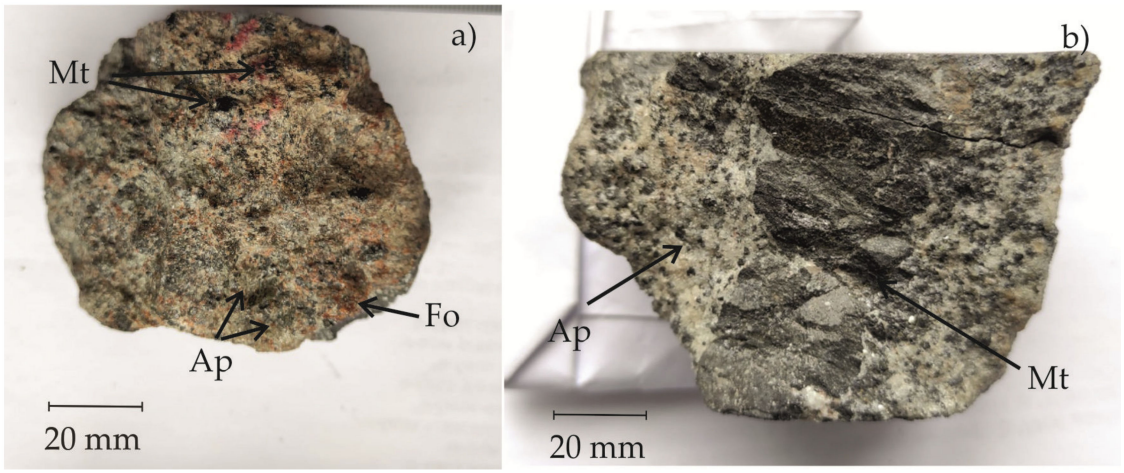


Figure 2. (**a**) baddeleyite-containing phoscorite. (**b**) pyrochlore containing phoscorite (Mt—magnetite; Ap—apatite; Fo—forsterite).

Phoscorites of the FOS 2 group are medium-coarse-grained up to pegmatite rocks. Large grains of magnetite form intergrowths with each other, creating a banded structure. The rock consists of magnetite (45–50%), apatite (40–45%), phlogopite (up to 5%), olivine (up to 5%), and carbonates (up to 3%). Accessory minerals (<1%) are pyrochlore, baddeleyite, stronadelphite, barite, galena, chalcopyrite, and pyrite. Magnetite forms sub-idiomorphic grains or irregular grains, the size of which can reach 4 cm. Magnetite grains contain many inclusions of other minerals, such as apatite, phlogopite, and pyrochlore. Apatite mainly forms idiomorphic-sub to idiomorphic grains up to 2 mm in size. However, it can also form idiomorphic inclusions up to 20 mcm in pyrochlore grains, while these grains form intergrowths with stronadelphite (Figure 3e). Phlogopite consists of lamellar idiomorphic grains up to 3–4 mm of a pale green color, widespread throughout the rock (Figure 3b). A smaller quantity of olivine is present in FOS 2 compared to FOS 1. This mineral is represented by sub-idiomorphic orange grains up to 1 mm in size and is still ubiquitous in the rock. Carbonates are represented by dolomite and calcite and are distributed in pockets between magnetite grains. Barite and sulfides are found throughout the rock. Pyrochlores are present in two textural varieties. The first variety forms rather large (up to 300 mcm) zoned well-faceted idiomorphic grains found in pockets between large grains of magnetite that form clusters. The core of most of these grains consists of idiomorphic prismatic baddeleyite grains with a size of 20–100 mcm. (Figure 3f). Such pyrochlore also contains inclusions of apatite, stronadelphite, and galena. The second variety of pyrochlores forms sub-idiomorphic grains, 40–50 microns in size, in inclusions in large grains of magnetite. These grains can be either zoned or homogeneous.

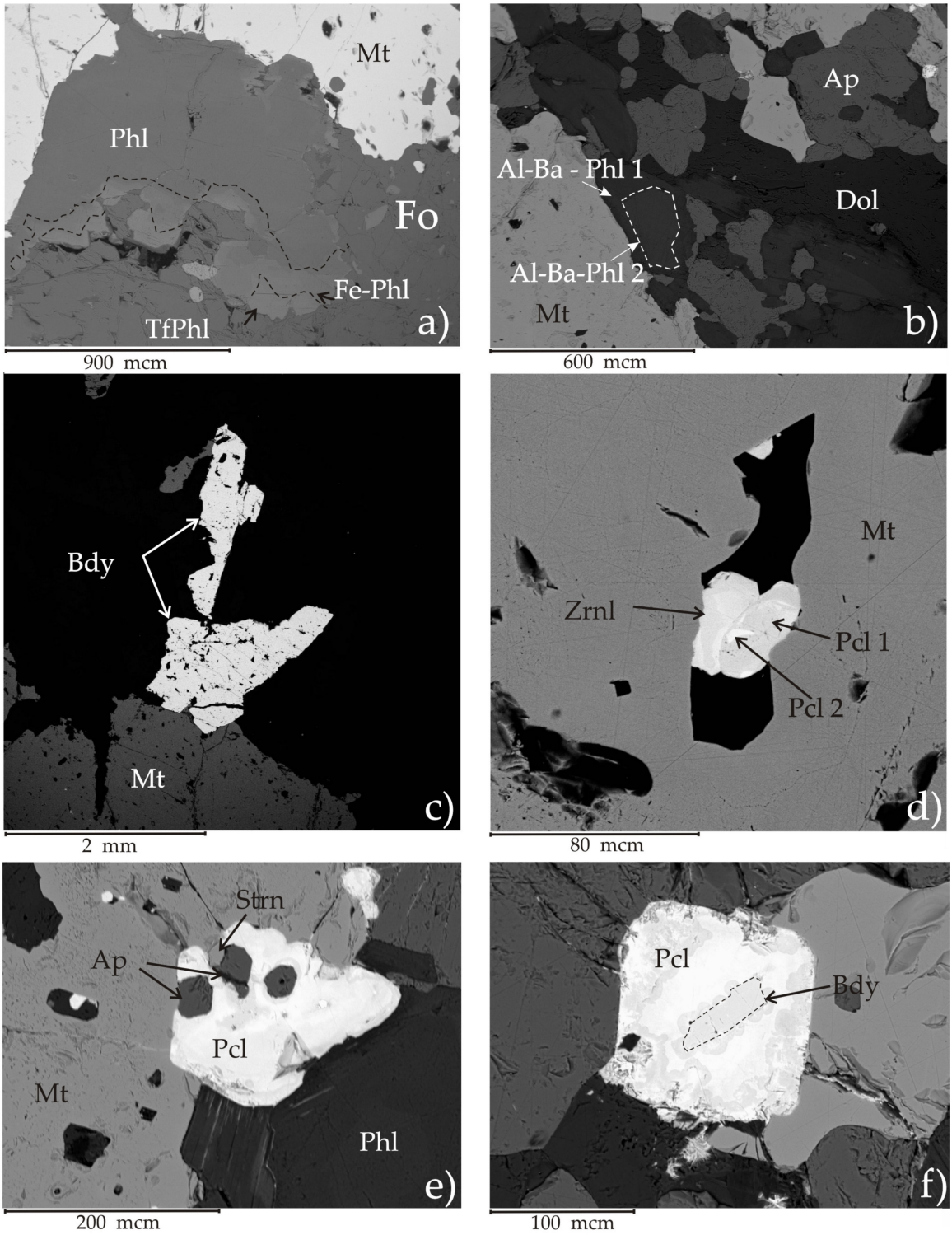


Figure 3. (**a**) The main grain of phlogopite (Phl) FOS 1, the edges of which pass into tetraferriflogopite (TfPhl) through the intermediate phase (Fe-Phl); (**b**) phlogopite FOS 2, the core of the grain is enriched in Ba (Al-Ba-Phl 1) compared to the edge (Al-Ba Phl 2), the whole grain is enriched in Al and Ba; (**c**) sub-idimorphic corroded grains of baddeleyite (Bdy) FOS 1; (**d**) the inclusion of zirconolite (Zrnl) and pyrochlore (Pcl 1 and Pcl 2) in magnetite FOS 1; (**e**) the inclusion of apatite and stronadelphite (Strn) in the pyrochlore (Pcl) grain FOS 2; (**f**) zonal pyrochlore grain (Pcl), in the core of which is the inclusion of baddeleyite (Bdy) FOS 2 (Mt—magnetite; Fo—forsterite; Ap—apatite; Dol—dolomite).

4.2. Mineral Chemistry

Magnetite and ilmenite Selected representative electron microprobe analyses of magnetite and ilmenite from the phoscorites of the Arbarastakh massif are presented in Table 1. Figure 4a shows that the Al concentration in magnetite is low (no more than 0.16 apfu—atoms per formula unit.) and is virtually the same for all phoscorites. The Mn concentration is also low and is in a narrow range (0.03–0.04 apfu.). In contrast, the Mg concentration increases from FOS 1 (0.01–0.02 apfu.) to FOS 2 (0.022–0.03 apfu.). The Fe^{3+} concentration is higher in FOS 2 compared to FOS 1 (up to 1.95 apfu.). The concentration of Ni and Cr in magnetites is extremely insignificant and often does not exceed the detection limit.

Table 1. Representative compositions of magnetite and ilmenite from the phoscorites of the Arbarastakh massif. b.d. = below the detection limit. The structural formulae of magnetite are calculated to three cations.

Unit	**FOS 1 Mt**			**FOS 2 Mt**			**FOS 1 Ilm**		
Sample	**50-3/13**	**50-3/19**	**50-3/20**	**53-3/12**	**53-3/13**	**53-3/14**	**50-3/2**	**50-3/5**	**50-3/6**
MgO	2.44	2.02	3.57	5.15	4.70	4.20	15.87	9.54	4.33
Al_2O_3	0.16	0.12	2.22	3.77	0.52	0.70	0.11	0.08	b.d.
TiO_2	2.33	2.05	2.53	0.36	0.38	0.60	58.17	55.07	51.07
Cr_2O_3	0.01	b.d.	0.02	b.d.	b.d.	b.d.	0.03	b.d.	b.d.
FeO	87.02	87.11	83.45	85.23	86.50	86.91	18.37	23.54	17.06
SiO_2	b.d.	0.04	0.03	0.01	b.d.	0.00	0.00	0.04	0.01
NiO	b.d.	0.02	0.02	b.d.	0.01	0.00	b.d.	b.d.	b.d.
MnO	1.09	1.03	1.09	1.11	1.10	1.08	6.21	9.70	23.58
V_2O_3	0.06	0.08	0.07	0.06	0.03	0.05	b.d.	b.d.	b.d.
ZnO	0.15	0.11	0.25	0.45	0.04	0.15	0.05	0.07	b.d.
Total	93.26	92.58	93.25	96.13	93.29	93.69	98.79	98.03	96.05
Fe^{3+}	1.852	1.864	1.749	1.817	1.952	1.930	0.012	0.018	0.057
Ti	0.066	0.059	0.071	0.010	0.011	0.017	0.992	0.989	0.971
Cr	0.000	-	0.001	-	-	-	0.000	-	-
Si	-	0.001	0.001	0.000	-	0.000	0.000	0.001	0.000
Al	0.007	0.006	0.097	0.157	0.023	0.030	0.003	0.002	-
Ni	-	0.001	0.001	-	0.000	0.000	-	-	-
V	0.002	0.002	0.002	0.002	0.001	0.001	-	-	-
Fe^{2+}	0.896	0.916	0.840	0.699	0.719	0.752	0.337	0.453	0.303
Mn	0.035	0.033	0.034	0.033	0.034	0.034	0.119	0.196	0.505
Zn	0.004	0.003	0.007	0.012	0.001	0.004	0.001	0.001	-
Mg	0.137	0.115	0.198	0.271	0.259	0.231	0.536	0.340	0.163
Total	3.000	3.000	3.000	3.000	3.000	3.000	2.000	2.000	2.000

Minerals of the ilmenite group are found only in FOS 1 and are represented by three different mineral species: ilmenite, geikielite, and pyrophanite. Ilmenite and geikielite have extremely similar chemical compositions; the total Fe concentration varies from 0.35 to 0.47 apfu., the Mg concentration ranges from 0.34 to 0.54 apfu. The Mn concentration in geikielite is about 0.12 apfu., while in ilmenite, it is 0.19–0.2 apfu. Pyrophanite contains a large amount of total Fe (0.36–0.4 apfu.) and Mg (0.16–0.195 apfu.) and is distinguished as a separate mineral species only by the main component, Mn, the concentration of which is 0.456–0.505 apfu.

Apatite Selected representative electron microprobe analyses of apatite from the phoscorites of the Arbarastakh massif are presented in Table 2. Despite the large variety of textures, apatites within one group do not significantly differ in chemical composition. The Cl concentrations are very low, typical of carbonatites and related rocks [30–32]. In general, apatite from phoscorite tends to change in composition with an increase in F from FOS 1 (from 0.35 to 0.45 apfu.) to FOS 2 (from 0.45 to 0.6 apfu.) (Figure 5d), which may reflect the transition from early hydroxylapatite to late fluorapatite as described in some works [14,15,33,34], at later stages of the development of the system. Similar behavior is seen for Sr with an increase in concentration from FOS 1 (from 0.03 apfu.) to FOS 2 (up

to 0.05 apfu.) (Figure 5a). The concentration of REE, on the contrary, slightly decreases from FOS 2 (0.015–0.025 apfu.) to FOS 1 (0.020–0.050 apfu.) (Figure 5b). The same trend is observed for Si (FOS 1: 0.01 to 0.065 apfu., for FOS 2, it does not exceed 0.015 apfu.) (Figure 5c). A 1:1 substitution of Ca + P ⇔ Si + REE on britholite is permissible. The apatites in FOS 2, which make up the volume of the rock, represent a separate group in this isomorphic series with Si and REE contents below the detection limit. The concentration of Na in phoscorites apatites is insignificant and varies from 0.015 to 0.05 apfu. The Ba, Mg, Cl, and S concentrations are either below the detection limit or do not exceed 0.01 apfu.

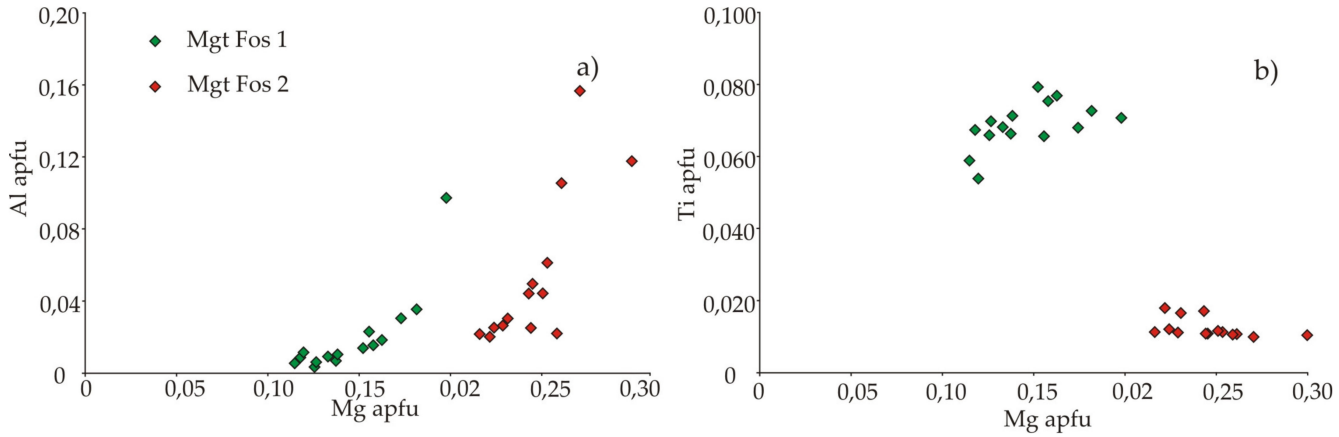


Figure 4. Variation of magnetite compositions from Arbrastakh phoscorites (**a**) Al, (**b**) Ti versus Mg.

Table 2. Representative compositions of apatite from phoscorites of the Arbarastakh massif. B.d. = below the detection limit. The structural formulae of apatite are calculated for eight cations (in table incl—inclusion).

Unit	**50-3 Main**		**50-3 Incl**		**53-3 Main**		**53-3 Incl**	
Sample	**50-3/1**	**50-3/2**	**50-3/12**	**50-3/13**	**53-1/1**	**53-1/2**	**53-3/12**	**53-3/15**
SiO_2	0.35	0.13	0.22	0.14	0.02	0.04	0.13	0.14
FeO	0.30	0.32	0.12	0.11	0.04	0.08	0.03	0.05
MgO	b.d.	b.d.	b.d.	b.d.	b.d.	b.d.	b.d.	b.d.
SrO	0.54	0.69	0.54	0.71	0.67	0.72	0.62	0.71
CaO	54.45	54.44	54.31	54.67	54.96	54.50	54.56	54.40
Na_2O	0.09	0.20	0.10	0.14	0.12	0.16	0.23	0.25
P_2O_5	40.71	40.99	41.06	41.55	41.55	41.59	40.90	40.71
SO_3	0.05	0.01	0.02	0.01	0.04	b.d.	0.03	0.02
BaO	0.03	b.d.	0.04	0.04	b.d.	0.01	0.05	0.00
Y_2O_3	0.02	0.03	0.06	0.08	0.03	0.02	0.04	0.03
La_2O_3	0.16	0.18	0.10	0.13	0.05	0.06	0.11	0.04
Ce_2O_3	0.38	0.32	0.36	0.29	0.16	0.23	0.26	0.28
Nd_2O_3	0.08	0.16	0.22	0.28	0.14	0.15	0.16	0.16
F	1.43	1.54	1.45	1.48	2.03	2.02	2.11	1.92
Cl	0.01	0.01	b.d.	0.01	0.01	0.00	b.d.	b.d.
Total	98.60	99.02	98.60	99.63	99.81	99.59	99.22	98.71
Ca	4.957	4.939	4.949	4.934	4.965	4.937	4.961	4.959
Fe^{2+}	0.02	0.02	0.01	0.01	0.00	0.01	0.00	0.00
Mg	-	-	-	-	-	-	-	-
Sr	0.027	0.034	0.027	0.035	0.033	0.035	0.031	0.035
Na	0.015	0.033	0.016	0.022	0.020	0.027	0.038	0.041

Table 2. *Cont.*

Unit	50-3 Main		50-3 Incl		53-3 Main		53-3 Incl	
Sample	**50-3/1**	**50-3/2**	**50-3/12**	**50-3/13**	**53-1/1**	**53-1/2**	**53-3/12**	**53-3/15**
Ba	0.001	-	0.001	0.001	-	0.000	0.001	0.000
Y	0.001	0.002	0.003	0.004	0.001	0.001	0.002	0.001
La	0.005	0.006	0.003	0.004	0.001	0.002	0.003	0.001
Ce	0.012	0.010	0.011	0.009	0.005	0.007	0.008	0.009
Nd	0.002	0.005	0.007	0.008	0.004	0.005	0.005	0.005
Total A	5.042	5.050	5.025	5.025	5.032	5.020	5.051	5.055
P	2.929	2.939	2.956	2.963	2.966	2.977	2.938	2.933
Si	0.03	0.01	0.02	0.01	0.00	0.00	0.01	0.01
Total Z	2.96	2.95	2.98	2.98	2.97	2.98	2.95	2.94
Total	8.00	8.00	8.00	8.00	8.00	8.00	8.00	8.00
F	0.383	0.413	0.389	0.393	0.541	0.539	0.567	0.518
S	0.003	0.001	0.001	0.001	0.002	-	0.002	0.001
Cl	0.001	0.001	-	0.002	0.001	0.000	-	-
OH	0.616	0.586	0.611	0.605	0.458	0.460	0.433	0.482
Total Y	1.003	1.001	1.001	1.001	1.002	1.000	1.002	1.001

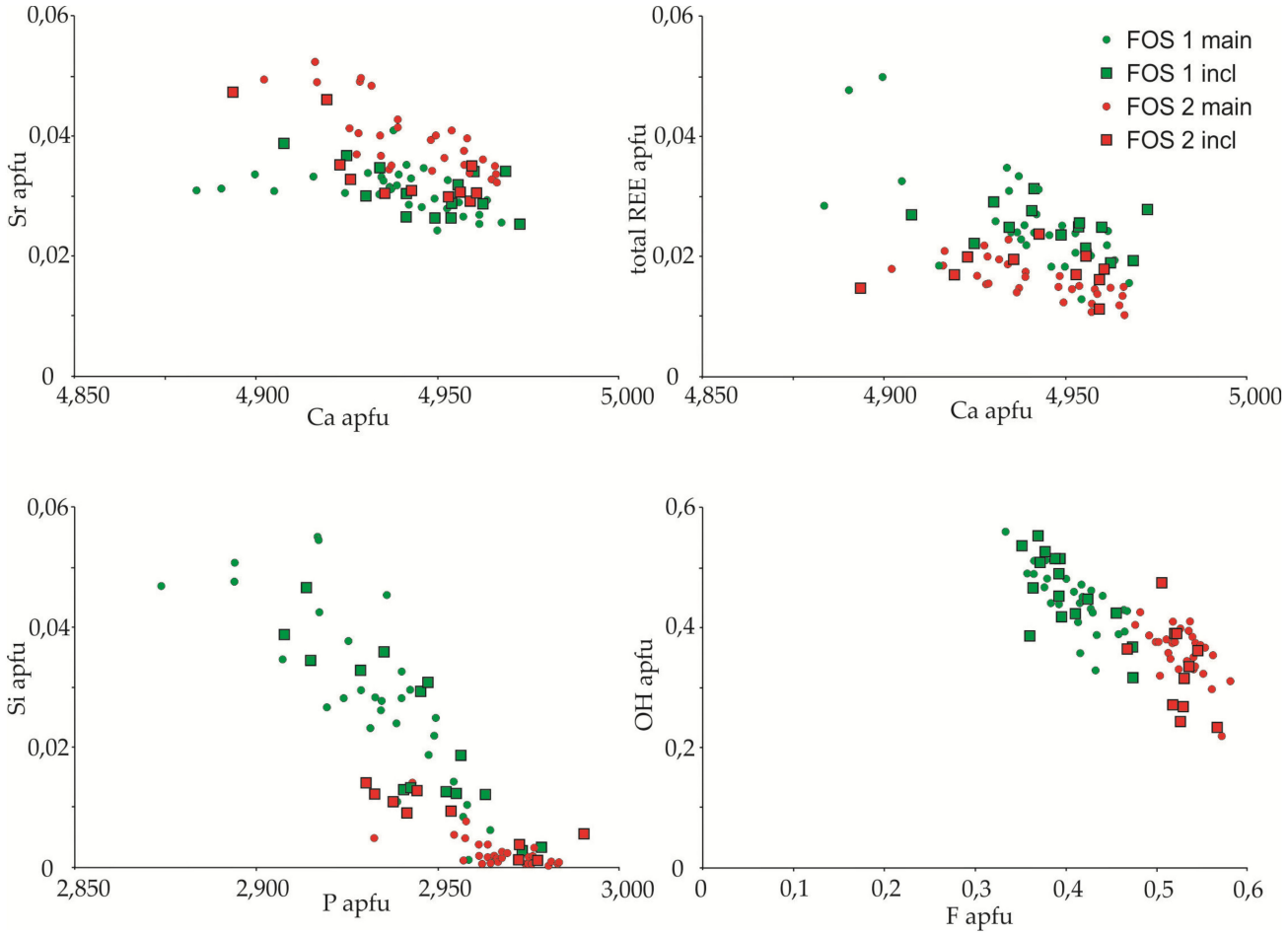


Figure 5. Compositional variation of apatite from Arbrastakh phoscorites (**a**) Ca vs. Sr (**b**) Ca vs. REE; (**c**) P vs. Ti, (**d**) F vs. OH.

Phlogopite Selected representative electron microprobe analyses of phlogopite from the phoscorites of the Arbarastakh massif are presented in Table 3. Mica in FOS 1 is represented by the phlogopite–tetraferriphlogopite series due to the gradual replacement

of Al^{3+} by Fe^{3+} in the tetrahedral position from the grain core to its edge. The concentration of Fe^{3+}, calculated according to the method described by Brod et al. [28], can range from 0.1 apfu. in the core (with the corresponding Al concentration of 1.1 apfu.), up to 1.015 apfu. in the border of the grain (Al at 0.015 apfu.). The concentrations of Mg and Fe^{2+} for these micas are constant. In addition, the concentration of Ti remains constant in the phlogopites of FOS 1. For tetraferriphlogopite, the concentration does not exceed 0.002 apfu., and for the unchanged phlogopites in FOS 1, it can reach 0.01 apfu. (Figure 6a). The Na concentration is insignificant and varies from 0.03 to 0.06 apfu. (Figure 6b).

Table 3. Representative compositions of phlogopite from the phoscorites of the Arbarastakh massif. B.d. = below the detection limit. The structural formulae of micas are calculated for seven cations (Z + B).

Unit	FOS 1 Incl		FOS 1 Core		FOS 1 Mid		FOS 1 Ring		FOS 2 Core		FOS 2 Ring	
Sample	**50-3/1**	**50-3/16**	**50-3/2**	**50-3/5**	**50-3/7**	**50-3/8**	**50-3/43**	**50-3/44**	**53-3/9**	**53-3/10**	**53-3/3**	**53-3/4**
SiO_2	41.00	39.69	42.34	41.48	42.56	41.15	40.22	40.38	36.74	35.98	38.08	38.31
TiO_2	0.11	0.11	0.03	0.06	0.01	0.03	b.d.	0.01	0.15	0.19	0.12	0.10
Al_2O_3	11.64	10.52	10.78	10.00	8.57	8.64	1.15	2.30	16.51	17.08	16.21	15.66
FeO	3.09	3.35	3.57	4.52	6.58	6.65	16.35	15.06	1.94	2.08	2.09	1.91
MgO	26.89	25.81	28.00	27.57	27.83	27.60	26.70	26.58	25.81	25.45	26.86	26.46
CaO	0.01	0.04	b.d.	b.d.	b.d.	b.d.	b.d.	b.d.	b.d.	b.d.	b.d.	b.d.
MnO	0.04	0.05	0.04	0.06	0.07	0.07	0.13	0.11	0.05	0.05	0.03	0.05
SrO	b.d.	b.d.	b.d.	b.d.	b.d.	b.d.	b.d.	b.d.	b.d.	b.d.	b.d.	b.d.
BaO	0.24	0.14	0.18	0.11	0.01	b.d.	0.05	0.03	4.23	4.81	2.20	2.06
Na_2O	0.43	0.40	0.26	0.23	0.25	0.28	0.37	0.36	0.15	0.31	0.21	0.14
K_2O	10.49	10.68	10.69	10.53	10.45	10.59	9.86	9.98	9.34	8.76	9.63	10.07
F	0.45	0.32	0.29	0.51	0.36	0.37	0.25	0.26	0.87	1.08	0.99	0.83
Cl	0.20	0.21	0.02	0.02	0.01	0.01	0.01	b.d.	0.00	0.01	0.02	b.d.
Total	94.57	91.32	96.19	95.10	96.69	95.37	95.10	95.06	95.79	95.79	96.43	95.58
Na	0.060	0.059	0.035	0.032	0.035	0.039	0.053	0.052	0.021	0.043	0.029	0.019
K	0.960	1.020	0.956	0.957	0.936	0.963	0.925	0.934	0.865	0.815	0.868	0.918
Ca	0.001	0.003	-	-	-	-	-	-	-	-	-	-
Ba	0.007	0.004	0.005	0.003	0.000	-	0.002	0.001	0.120	0.137	0.061	0.058
Total A	1.028	1.086	0.996	0.993	0.971	1.002	0.980	0.987	1.007	0.995	0.957	0.995
Mn	0.002	0.003	0.002	0.003	0.004	0.004	0.008	0.007	0.003	0.003	0.002	0.003
Mg	2.878	2.881	2.927	2.929	2.913	2.936	2.927	2.908	2.792	2.767	2.829	2.820
Fe^{2+}	0.104	0.187	0.043	0.022	0.043	0.000	0.004	0.037	0.007	-	-	-
Fe^{3+}	0.081	0.023	0.167	0.248	0.344	0.396	1.002	0.887	0.111	0.124	0.109	0.087
Al	0.985	0.928	0.891	0.840	0.709	0.727	0.100	0.199	1.412	1.468	1.349	1.319
Si	2.943	2.972	2.969	2.955	2.988	2.936	2.959	2.963	2.667	2.624	2.690	2.738
Ti	0.006	0.006	0.002	0.003	0.000	0.001	-	0.001	0.008	0.010	0.006	0.005
Total B + Z	7.000	7.000	7.000	7.000	7.000	7.000	7.000	7.000	7.000	7.000	7.000	7.000
Total	8.028	8.086	7.996	7.993	7.971	8.002	7.980	7.987	8.007	7.995	7.957	7.995
OH	1.875	1.897	1.933	1.882	1.919	1.915	1.940	1.940	1.800	1.750	1.775	1.812
F	0.101	0.076	0.065	0.115	0.080	0.083	0.059	0.060	0.200	0.249	0.222	0.188
Cl	0.024	0.026	0.002	0.002	0.001	0.001	0.001	-	0.000	0.001	0.003	-
Total Y	2.000	2.000	2.000	2.000	2.000	2.000	2.000	2.000	2.000	2.000	2.000	2.000

Phlogopites from FOS 2 show enrichment in Al and Ba due to two replacement mechanisms:

$K^+ + Si^{4+} \Leftrightarrow Ba^{2+} + Al^{3+}$ replacement of phlogopite with kinoshitalite;

$Mg^{2+} + Si^{4+} \Leftrightarrow 2Al^{3+}$ replacement of phlogopite with eastonite.

The center of the grains is composed of the most saturated Al (up to 1.55 apfu.) and Ba (up to 0.15 apfu.) phlogopite. The outer parts have a significant component of eastonite (Al 1.45 apfu.); however, the kinoshitalite content is lower (Ba up to 0.07 apfu.) (Figure 7a), and the amount of Si, accordingly, falls to 2.5 apfu. (Figure 7b). In addition, the concentrations of Ti and Na slightly decrease from the central part of the grain to the edge, from 0.012 to 0.005 apfu. and from 0.005 to 0.002 apfu., respectively. The concentration of F in FOS 2 is approximately equal in these micas, higher than in FOS 1, and ranges from 0.15 to

0.25 apfu. The Fe in FOS 2 phlogopite is most likely in a trivalent state, but it is impossible to determine its coordination state. The concentration of Mg in FOS 2 does not vary much across the crystal (2.75–2.85 apfu.). This confirms that the substitution from the edge to the center occurs according to the first mechanism described above since there is no change in Mg (Figure 7c). There is also a slight deficit of charge for these micas, which does not exceed 0.13 c.f.u.

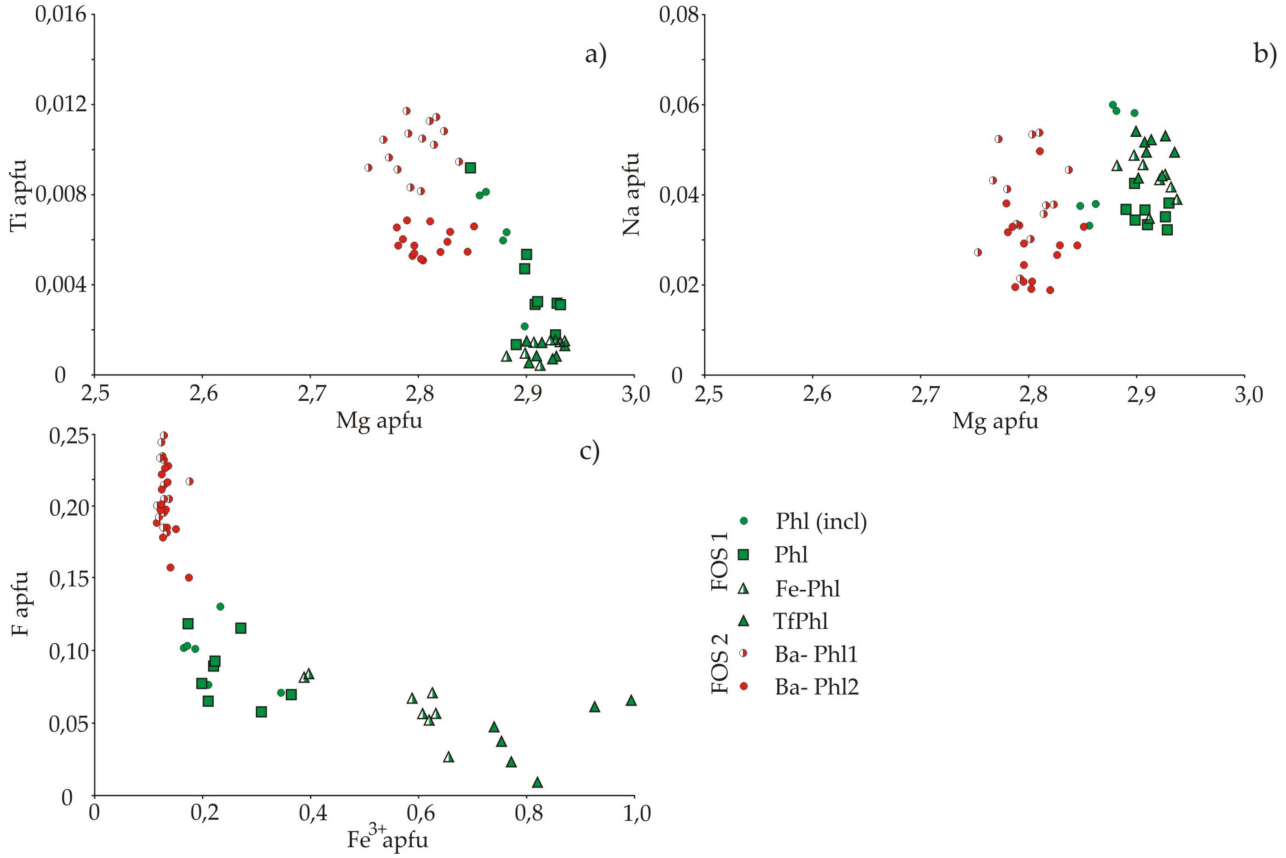


Figure 6. Variation of phlogopite compositions from Arbrastach phoscorites (**a**) Ti; (**b**) Na versus Mg, (**c**) shows a diagram of Fe^{3+}–F.

The F concentration decreases from 0.15 to 0.05 apfu. for the varieties more saturated in Fe^{3+} (Figure 6c), which is a typical feature of Fe-rich micas known as "Fe-F avoidance" [35]. In FOS 2 phlogopites, F varies from 0.15 to 0.25 apfu. An increase in the F concentration in phlogopites from earlier to later phases is characteristic of the carbonatite–phoscorite complexes of the world. For example, in the Palabora massif, the F concentration increases from carbonatites to phoscorites and subsequently to the late carbonatites that penetrate them [13]. The Cl concentration in micas from both types of phoscorites from Arbarastakh is generally low, no more than 0.001 apfu.

Baddeleyite and zirconolite Zirconium minerals in Arbarastakh phoscorites are represented by baddeleyite and zirconolite; selected representative electron microprobe analyses of baddeleyite and zirconolite from the phoscorites of the Arbarastakh massif are presented in Table 4. Baddeleyite is present in both types of phoscorite, but, as already mentioned, there are significant differences in the amount and the morphology of the grains. The chemical composition for different types of phoscorites varies slightly. Low concentrations of Fe (up to 0.01 apfu.), Nb, and Ta (up to 0.01 apfu. in total) are present in FOS 2 baddeleyite probably due to a close relationship with pyrochlore, in which baddeleyite is an inclusion. In addition, in FOS 1 baddeleyite (up to 0.008 to 0.01 apfu.), the concentration of Hf is

slightly higher than in FOS 2 (from 0.006 to 0.008 apfu.) The REE, Ti, Th, U, and others are present in insignificant amounts in the baddeleyites of both groups of phoscorites.

Table 4. Representative compositions of baddeleyite and zirconolite from the phoscorites of the Arbarastakh massif. B.d. = below the detection limit. Baddeleyite analyses were normalized to 100%. The structural formulae of baddeleyite are calculated for two oxygens; the structural formulae of zirconolite are calculated for 28 charges.

Unit	**FOS 1 Bdlt**			**FOS 2 Bdlt**			**FOS 1 Zrn**			
Sample	**50-3/9**	**50-3/21**	**50-3/36**	**53-3/15**	**53-3/16**	**53-3/18**	**50-3/1**	**50-3/4**	**50-3/5**	**50-3/23**
SiO_2	b.d.	b.d.	b.d.	b.d.	b.d.	b.d.	b.d.	0.01	b.d.	b.d.
TiO_2	0.03	0.05	0.05	0.03	0.00	0.04	16.83	14.09	16.24	16.55
FeO	0.01	0.03	0.09	0.24	0.44	0.26	8.21	8.22	9.23	9.84
MgO	b.d.	b.d.	0.02	0.07	0.37	0.28	0.80	0.72	0.71	0.43
CaO	0.04	0.03	0.04	0.06	0.06	0.05	8.36	9.12	9.34	10.92
SrO	0.03	b.d.	b.d.	b.d.	b.d.	b.d.	0.07	0.29	b.d.	0.08
MnO	0.02	0.02	b.d.	0.08	0.07	0.03	0.58	0.52	0.62	0.61
BaO	0.03	0.02	0.09	0.10	0.10	0.11	0.01	0.10	b.d.	0.03
Nb_2O_5	b.d.	b.d.	0.03	1.69	3.70	3.61	18.42	17.59	20.10	22.37
Ta_2O_5	b.d.	b.d.	0.10	0.21	0.53	0.68	0.91	6.46	1.30	1.23
ZrO_2	98.01	98.13	97.81	95.76	92.35	92.28	28.83	28.83	29.20	29.40
HfO_2	1.53	1.53	1.32	1.05	1.02	1.18	0.39	0.26	0.68	0.50
UO_2	0.02	0.00	0.06	b.d.	0.24	0.46	b.d.	b.d.	b.d.	b.d.
ThO_2	0.00	0.01	b.d.	0.11	0.16	0.17	0.07	0.26	b.d.	0.20
Sc_2O_3	0.14	0.16	0.30	0.55	0.68	0.75	b.d.	b.d.	b.d.	b.d.
Ce_2O_3	0.02	b.d.	0.03	b.d.	0.07	0.03	4.50	3.01	3.24	2.97
La_2O_3	0.03	b.d.	0.02	b.d.	0.02	b.d.	0.81	0.48	0.45	0.56
Pr_2O_3	b.d.	b.d.	b.d.	0.04	0.07	b.d.	1.21	0.81	0.89	0.58
Nd_2O_3	0.09	0.02	0.05	0.00	0.11	0.07	5.16	4.28	4.47	2.30
Total	100.00	100.00	100.00	100.00	100.00	100.00	95.15	95.06	96.47	98.57
Mg	-	-	0.001	0.002	0.011	0.009	0.165	0.152	0.142	0.084
Ca	0.001	0.001	0.001	0.001	0.001	0.001	1.236	1.375	1.352	1.526
Sr	0.000	-	-	-	-	-	0.006	0.024	-	0.006
Mn	0.000	0.000	-	0.001	0.001	0.001	0.068	0.062	0.071	0.067
Ba	0.000	0.000	0.001	0.001	0.001	0.001	0.001	0.006	-	0.002
Sc	0.003	0.003	0.005	0.010	0.012	0.013	-	-	-	-
Ce	0.000	-	0.000	-	0.001	0.000	0.227	0.155	0.160	0.142
La	0.000	-	0.000	-	0.000	-	0.041	0.025	0.023	0.027
Pr	-	-	-	0.000	0.001	-	0.061	0.041	0.044	0.028
Nd	0.001	0.000	0.000	0.000	0.001	0.001	0.254	0.215	0.215	0.107
Total A	-	-	-	-	-	-	2.058	2.054	2.007	1.988
Zr	0.987	0.987	0.984	0.957	0.919	0.920	1.939	1.978	1.923	1.869
Hf	0.009	0.009	0.008	0.006	0.006	0.007	0.015	0.011	0.026	0.018
U	0.000	0.000	0.000	_-	0.001	0.002	-	-	-	-
Th	0.000	0.000	-	0.001	0.002	0.002	0.004	0.018	-	0.013
Total B	-	-	-	-	-	-	1.958	2.006	1.949	1.900
Si	-	-	-	-	-	-	-	0.001	-	-
Ti	0.001	0.001	0.001	0.000	0.000	0.001	1.746	1.491	1.649	1.623
Fe	0.000	0.001	0.002	0.004	0.007	0.004	0.947	0.968	1.043	1.073
Nb	-	-	0.000	0.017	0.037	0.036	1.249	1.217	1.335	1.434
Ta	-	-	0.001	0.001	0.003	0.004	0.036	0.259	0.050	0.046
Total C	-	-	-	-	-	-	3.978	3.934	4.077	4.176
Total	0.997	0.998	0.995	0.987	0.976	0.976	7.894	7.947	7.975	7.977

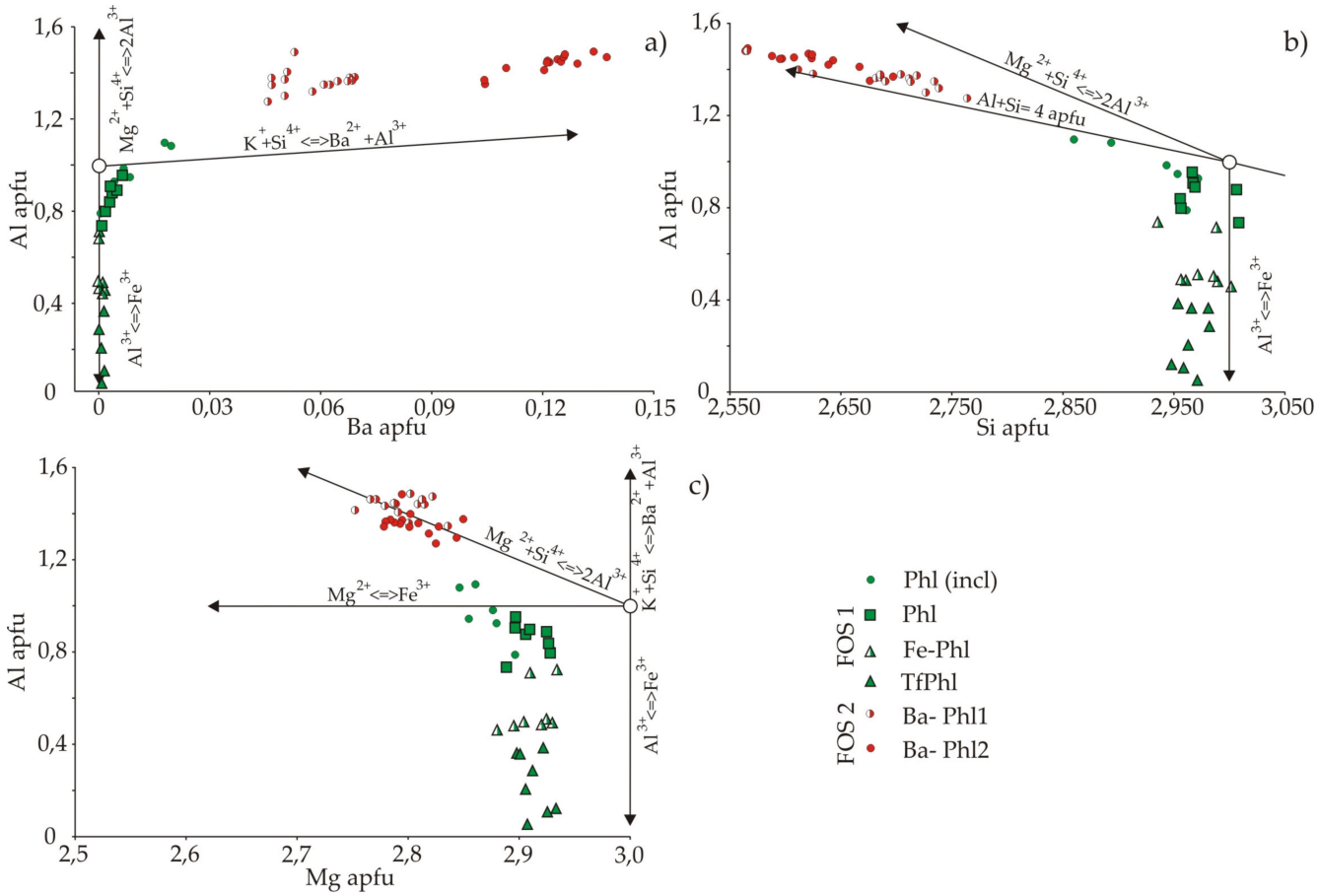


Figure 7. Variations in phlogopite compositions from Arbrastach phoscorites (**a**) Ba; (**b**) Si; (**c**) Mg versus Al. Zirconolite is present only in FOS 1, and its chemical composition differs from the empirical formula, $CaZrTi_2O_7$. Although naturally occurring zirconolites may be rich in Nb and Ta [36], the analyses in Table 4 are specifically adjusted for the laachite formula to show the similarity of the chemical composition of the zirconolites to this mineral described by Chukanov and others [37]. The concentration of Nb + Ta is high (1.28 to 1.48 apfu.) and in some cases can equal Ti (1.50 to 1.75 apfu.). The zirconolite also contains REE, mainly Ce and Nd (total REE 0.30–0.58 apfu.). It is difficult to give an exact name to this mineral since Fe is absent in the zirconolite formula presented in The New IMA List of Minerals (January 2021). However, in many crystallographic studies of Nb-rich zirconolites [38,39], a separate position M5 for Fe is distinguished in the "doubled" formula of zirconolite (the center is a pentagonal polyhedron that separates the edges with an octahedron).

Pyrochlore Selected representative electron microprobe analyses of pyrochlore from the phoscorites of the Arbarastakh massif are presented in Table 5. The chemical composition of the pyrochlores is very different, both in the different groups of phoscorites and for different varieties of pyrochlore within a group.

For FOS 1, one variety was identified. It occurs in the form of inclusions up to 50 mcm in size in magnetite and baddeleyite grains. This pyrochlore is closest to the reference formula for fluornatropyrochlore according to the nomenclature [29]. The Na and Ca concentrations are approximately 1.0 apfu. for each element; Na predominates slightly (Figure 8a). The concentration of Ta replacing Nb (1.4–1.8 apfu.) is usually insignificant, and only in some zones can it reach 0.2 apfu. (Figure 8b). The concentration of F (0.5–1 apfu.) dominates over OH (Figure 9b). Increased concentrations of Ti (0.15–0.25 apfu.) and LREE (0.1–0.14 apfu.) are also observed (Figure 10a).

Table 5. Representative compositions of pyrochlore from phoscorites in the Arbarastakh massif. B.d. = below the detection limit. The structural formulae of pyrochlore are calculated for two cations (B).

Unit	**FOS 1 Incl**		**FOS 2 Incl**		**FOS 2 Core**		**FOS 2 Ring**	
Sample	**50-5**	**50-6**	**53-31**	**53-33**	**53-56**	**53-57**	**53-62**	**53-70**
SiO_2	0.17	0.04	0.29	0.35	0.18	0.37	0.25	0.13
TiO_2	5.16	4.82	0.47	0.16	0.44	0.50	0.42	0.81
Al_2O_3	b.d.	b.d.	0.11	0.00	0.15	0.01	0.06	0.06
FeO	2.29	1.85	3.76	3.97	2.52	3.04	3.03	2.47
MgO	b.d.	0.02	0.02	b.d.	0.16	0.20	0.14	0.15
CaO	15.06	15.87	12.95	13.38	7.11	8.63	8.01	8.18
BaO	0.03	0.02	0.09	b.d.	1.01	0.97	0.51	0.70
Na_2O	7.42	7.49	7.69	7.44	7.03	6.45	6.80	6.43
K_2O	0.04	0.03	0.04	0.03	0.06	b.d.	0.03	0.03
Nb_2O_5	49.02	58.82	43.94	39.27	47.99	46.38	47.47	45.07
Ta_2O_5	10.28	2.64	19.24	27.13	4.24	3.61	4.70	9.42
ZrO_2	1.25	0.73	1.65	2.07	3.31	4.31	3.41	3.42
UO_2	b.d.	b.d.	0.22	0.03	7.62	5.90	8.24	4.52
ThO_2	0.42	0.01	3.22	2.02	10.45	12.01	9.19	11.14
Y_2O_3	b.d.	b.d.	b.d.	b.d.	b.d.	b.d.	b.d.	b.d.
Sc_2O_3	b.d.	b.d.	b.d.	b.d.	b.d.	b.d.	b.d.	b.d.
Ce_2O_3	3.50	2.90	1.17	1.27	1.60	1.73	1.66	1.94
La_2O_3	0.63	0.72	0.20	0.18	0.32	0.27	0.28	0.27
Pr_2O_3	0.22	0.34	0.00	0.26	0.15	0.18	0.17	0.14
Nd_2O_3	0.98	0.74	0.38	0.40	0.86	0.87	0.89	0.96
SrO	0.99	0.71	0.80	0.78	1.36	1.26	1.87	2.03
PbO	0.18	0.04	b.d.	b.d.	0.44	0.35	0.03	0.21
F	4.41	4.81	3.68	3.82	2.72	2.53	2.78	2.88
Total	100.20	100.56	98.38	100.93	98.56	98.51	98.78	99.74
Na	0.858	0.826	0.940	0.909	0.929	0.850	0.890	0.844
K	0.003	0.002	0.003	0.002	0.005	-	0.002	0.003
Ca	0.960	0.964	0.871	0.901	0.517	0.626	0.578	0.592
Ba	0.001	0.000	0.002	-	0.027	0.026	0.014	0.019
Sr	0.034	0.023	0.029	0.028	0.054	0.050	0.073	0.080
Y	-	-	-	-	-	-	-	-
Sc	-	-	-	-	-	-	-	-
Ce	0.076	0.060	0.027	0.029	0.040	0.043	0.041	0.048
La	0.014	0.015	0.005	0.004	0.008	0.007	0.007	0.007
Pr	0.005	0.007	0.000	0.006	0.004	0.005	0.004	0.003
Nd	0.021	0.015	0.009	0.009	0.021	0.021	0.021	0.023
Pb	0.003	0.001	-	-	0.008	0.006	0.001	0.004
U	-	-	0.003	0.000	0.115	0.089	0.123	0.068
Th	0.012	0.000	0.099	0.062	0.346	0.397	0.301	0.367
Total A	1.988	1.914	1.988	1.950	2.074	2.119	2.055	2.058
Nb	1.434	1.640	1.357	1.213	1.603	1.545	1.570	1.497
Ta	0.174	0.043	0.344	0.485	0.082	0.070	0.090	0.181
Mg	-	0.002	0.002	-	0.016	0.020	0.014	0.015
Fe^{3+}	0.114	0.088	0.197	0.209	0.143	0.172	0.171	0.140
Si	0.010	0.002	0.018	0.022	0.012	0.025	0.017	0.009
Ti	0.231	0.206	0.022	0.008	0.022	0.025	0.021	0.041
Al	-	-	0.008	0.000	0.012	0.001	0.005	0.005
Zr	0.036	0.020	0.050	0.063	0.110	0.142	0.112	0.113
Total B	2.000	2.000	2.000	2.000	2.000	2.000	2.000	2.000
Total	3.988	3.914	3.988	3.950	4.074	4.119	4.055	4.058
F	0.831	0.863	0.731	0.758	0.585	0.541	0.591	0.616

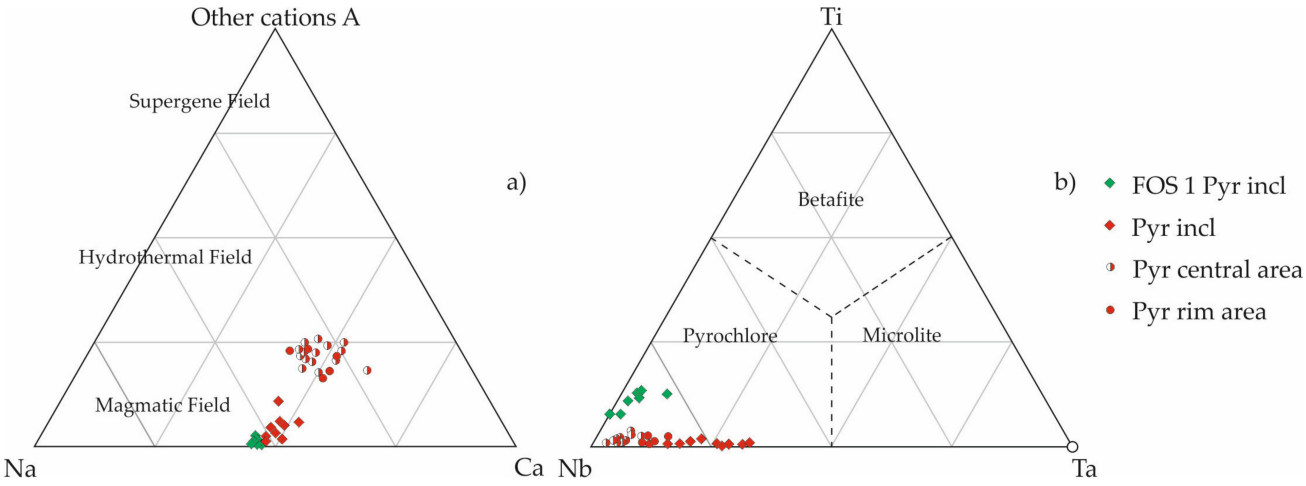


Figure 8. Variations in the chemical composition of pyrochlore in the Arbarastakh massif (**a**) position A (according to [42]), (**b**) position B.

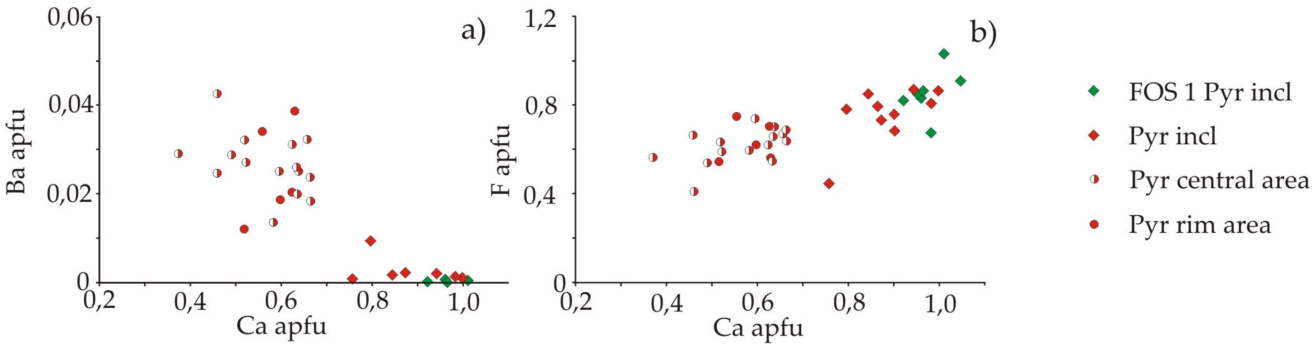


Figure 9. Variation of pyrochlore compositions from Arbrastakh phoscorites (**a**) Ba; (**b**) F vs. Ca.

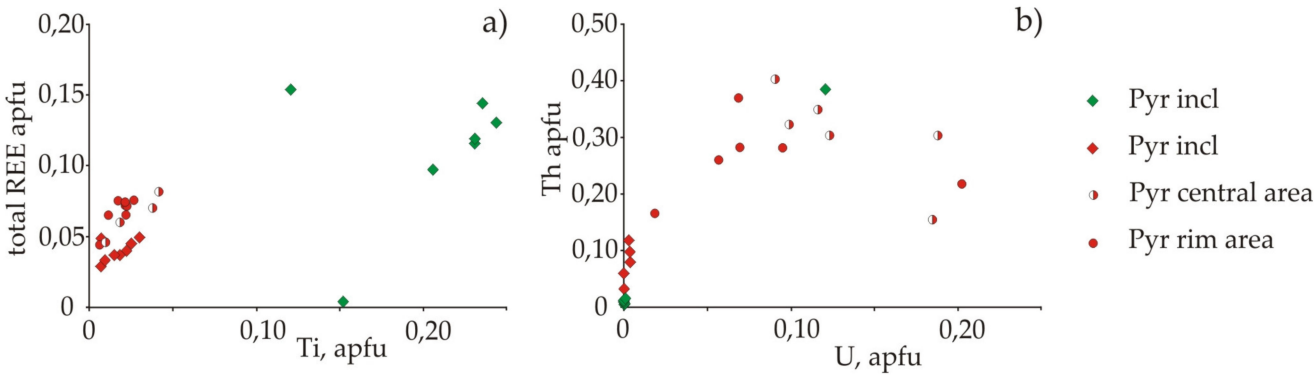


Figure 10. Variation of pyrochlore compositions from Arbrastakh phoscorites (**a**) REE vs. Ti; (**b**) Th vs. U.

Pyrochlore inclusions in magnetite in FOS 2 have affinities with the microlite composition due to the gradual replacement of Nb (1.5–1.9 apfu.) by Ta (0.30–0.50 apfu.) (Figure 8b). It is also worth noting that these grains are characterized by low contents of Fe (0.10–0.27 apfu.), which is in position B, and probably has an oxidation state of +3 to compensate the charge deficiency. Another characteristic feature of these pyrochlores is the low concentrations of Th, U, and Zr. In large zoned pyrochlore grains, those are located in pockets between massive magnetite grains, and the concentrations of these elements are the most significant. The zoning of grains is not associated only with the difference in the concentration of Ta (0.1–0.3 apfu.), but also Th (0.2–0.4 apfu.), and, to a lesser extent, Si (this dependence is difficult to observe based on the analysis of spectra,

but it is much clearer in mono-element maps (Figure 11). In addition, the grain rims are often enriched with Ti, Na, Ba, and REE (for example, Ce). In addition, these grains are enriched in U (0.05–0.20 apfu., Figure 10b) and are lower in Ba (0.01–0.05 apfu., Figure 9a). The F content for FOS 2 pyrochlores is significant (0.4–0.8 apfu.), but when recalculating the formula according to the method proposed by Atencio and other [29], a significant excess of charge compared to the empirical formula is observed for the zoned grains. It is highly problematic to compensate for this with additional anions in the Y position (for example, OH). In addition, for most analyses, an overabundance of cations is noted for position A, although for pyrochlores containing a significant amount of Th [40] or U [41], a cation deficiency in this position is observed.

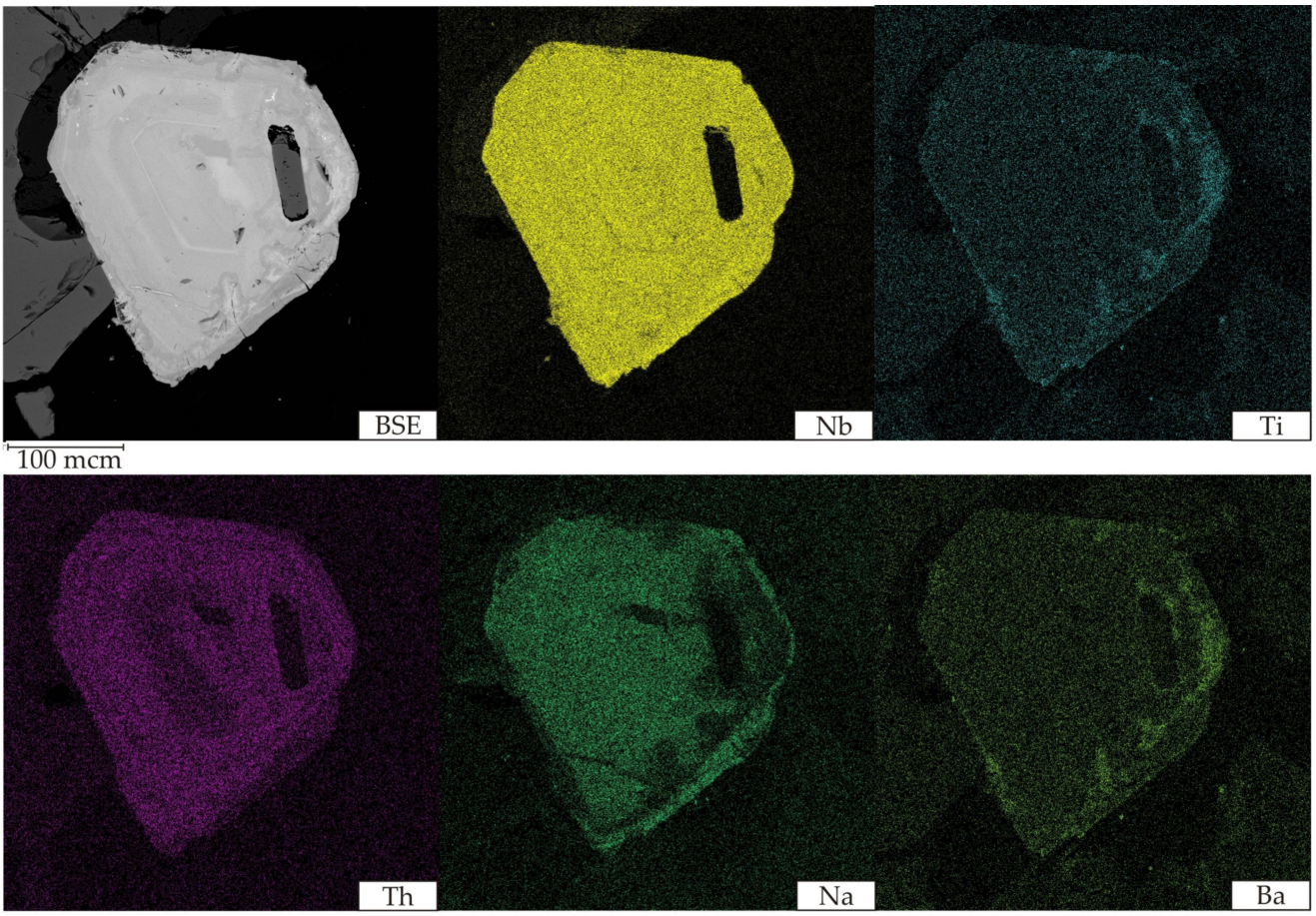


Figure 11. Monoelement maps of zonal grain in FOS 2 of the Arbarastakh massif (BSE—back scattering electorns).

5. Discussion

The origin of phoscorites is a currently unanswered question in the study of carbonatite complexes. The preferred theories are fractional crystallization and magma formation by separating its carbonatite melt as a result of liquation.

Geological observations indicate that the phoscorites of the Arbarastakh complex occur later than silicocarbonatites [23]. However, it is not currently possible to determine the sequence in which the two phoscorite types formed. The high percentage of olivine in FOS 1 (up to 30% by volume) suggests an earlier origin (since olivine is the highest-temperature mineral present), but the evolution of the chemical compositions of the studied minerals contains contradictions, discussed below.

5.1. Petrogenetic Evolution of Magnetite

Generally, the magnetite in the carbonatite–phoscorite complexes of the world is characterized by high concentrations of MgO and Al_2O_3, and the concentrations of Cr_2O_3, NiO are less than <0.02% [34]. For the Sokli complex, the magnetites in phoscorites of the early stage contain a large number of impurities, while for magnetite in the phoscorite late stage, the amount of Al, Mg, and Ti decreases [43]. In the Kovdor complex, Mg, Al, Ca, and V in magnetites increase from early to late phoscorites; Ti, Mn, Si, Cr, Zn, and Sc decrease [15]. The magnetites of the early phoscorites of the Salitre I massif are enriched in Ti, but the late phoscorites are enriched in Mg and Al. In this case, the authors have attributed this to the participation of different magmas for the phoscorites rather than the evolution of the melt [14]. If we assume the evolution of a single phoscorite system for the Arbarastakh complex, then the early crystallization of minerals of the mica and olivine group should lead to depletion of Mg and Al in the residual melt, which, in general, should lead to standard magnetite compositions for FOS 2. However, the Al, and much more significantly, Mg contents are higher in FOS 2. Thus, the observed changes in the chemical composition of magnetite indicate a contradiction with the sequence of formation of FOS 1 and FOS 2, as they have mineral compositions suggestive of both early and late origins.

5.2. Petrogenetic Evolution of Micas

Based on the results obtained, three types of phlogopite are distinguished in the phoscorites of Arbarastakh:

1. The phlogopite found in FOS 1, the chemical composition of which is most consistent with the empirical formula.
2. A phlogopite enriched in Fe^{3+}, which is gradually transforming into tetraferriphlogopite, found in FOS 1.
3. A phlogopite, enriched in Ba and Al (through substitution by the mechanisms described in Section 4.2), found in FOS 2. In addition, these micas are enriched in Ti and F relative to Type 1 and 2 micas.

Based on their textural appearance, the phlogopites of the first and third types are interpreted as products of orthomagmatic crystallization, while the rims of tetraferriphlogopite were formed during the late magmatic or hydrothermal stages. Generally, the increase in Fe in phlogopites is used to assess the evolution of the magmatic system [28]. However, co-crystallization of more magnetite (as in phoscorites or some carbonatites) causes an increase in the Mg relative to the Fe in phlogopites [44]. Experimental studies have shown that the melt/liquid composition (for example, the contents of O_2 and P) only slightly affects the mechanisms of Ti replacement in phlogopite, while a decrease in temperature or an increase in pressure (especially in rocks with high K) causes a much stronger decrease in Ti solubility [45]. The crystallization of Ti-containing phases (ilmenite and titanomagnetite) combined with a decrease in temperature should lead to depletion of Ti phlogopites during magma evolution [46,47]. However, although we observe the most saturated Ti magnetite in FOS 1, FOS 2 phlogopite contains a larger amount of Ti than FOS 1 phlogopite, which leads us to another contradiction.

Phlogopite enriched in Ba and Al is present only in FOS 2. While the grain edges are enriched only in eastonite, the center of the grain is most enriched in kinoshitalite. It is assumed that the FOS 2 magma was enriched in Ba and Al. This is partly confirmed by the increased concentration of Al in magnetite. There is an assumption that Ba enrichment may be caused by the differentiation of magma, when incompatible elements accumulate in large quantities in the residual liquid [44,48]. In addition, the highest concentrations of F are observed in phlogopites containing Ba. Experimental studies have shown that the F concentration in phlogopite increases with decreasing temperature, which is associated with an increase in the crystal:liquid ratio and is independent of pressure [45]. However, early crystallization of phlogopite in FOS 1 should have led to the depletion of the Al in the melt (and a subsequent increase in Fe in phlogopite); the assumption of an excess of aluminum in the residual melt is contradictory. Similar trends in the evolution of micas

are found in other carbonatite complexes [13,44,49,50] and were interpreted as a result of contamination by the host rock.

The Na concentration in phlogopites is generally used to indicate the degree of evolution of the melt. Typically, early crystallized phlogopites in carbonatites are depleted in sodium; later-stage phlogopites may contain significant amounts of Na [51]. However, this trend is not observed in the Arbarastakh phoscorites, and the decrease in K is associated with the replacement of Ba. Thus, the Na concentration increases from phlogopite to tetraferriphlogopite in FOS 1. This may be due to later magmatic or hydrothermal processes since Na has a high affinity for fluid phases [52]. For FOS 2, an increase in Na is characteristic of grains enriched with kinoshitalite.

Tetraferriphlogopite generally crystallizes as an orthomagmatic phase or from late-stage fluids. As previously described, tetraferriphlogopite overgrows earlier phlogopites, forming rims with abrupt compositional changes, for example, as described by Brod et al. [29]. Similar trends in the evolution of the composition of micas are observed during metasomatic processes and are associated with a highly alkaline medium and an increased oxygen fugacity. Phlogopite replacement textures confirm the metasomatic formation of tetraferriphlogopite. Similar textures can be seen, for example, in the Belaya Zima carbonatite complex, where phlogopite is overgrown with tetraferriphlogopite as a result of the activity of late hydrothermal fluids [53].

A similar set of micas is typical for many carbonatite deposits containing phoscorites, but most often, they do not appear together (Figure 12a). For example, the micas of the Palabora complex have a similar composition, where common phlogopite and representatives of the phlogopite–eastonite, phlogopite–kinoshitalite, and phlogopite–tetraferriphlogopite series are present [13]. Ba- and Al-enriched Palabora phlogopites occur in late carbonatites, intruding early banded carbonatites and phoscorites [54] (Figure 12b). The Jacupiranga phlogopites are enriched in Ba and Al, but their Ba concentrations are much higher than in the Palabora or Arbarastakh (up to 0.6 apfu.) phlogopites (Figure 12c). Jacupiranga phlogopite is depleted in Al during evolution, while in Palabora and Arbarastakh, evolution proceeds toward more Al-enriched phlogopites. The Sokli massif is characterized by the phlogopite–tetraferriphlogopite series and the phlogopite–eastonite mica series; however, barium-rich micas are absent (Figure 12d). The evolution of the composition of mica from phlogopite to tetraferriphlogopite is also characteristic of the phoscorites of Kovdor (Figure 12e). In general, it can be said that the composition of the micas of the phoscorites of the Arbarastakh massif is close to that of the Palabora micas. However, in terms of their textural appearance, the FOS 2 micas were enriched in Ba and Al and, in the course of post-magmatic metasomatism, approached the standard phlogopite.

5.3. Petrogenetic Evolution of Apatite

On the whole, apatite does not show large compositional variations between the phoscorites of Arbarastakh; nevertheless, there is a slight enrichment of the apatite components FOS 1 in Si and REE. In addition, there is an increase in the F concentration in the FOS 1 apatite compared to the FOS 2 apatite. An increase in the F content in apatites is generally interpreted by the process of fractional crystallization and indicates an increase in the concentration of volatile components during the evolution of melts. A similar tendency for F increase is noted in some alkaline complexes of the Kola Peninsula, northern Karelia, and the Oldoinyo Lengai volcano [55–57].

5.4. Petrogenetic Evolution of Accessory Minerals

As already noted, differences in the chemical composition are observed not only for the main minerals but also for the accessory minerals of the phoscorites. For FOS 1, there is a clear predominance of zirconium-containing phases (baddeleyite, zirconolite), and the amount of pyrochlore is significantly lower than in FOS 2. The baddeleyite has a chemical composition close to the empirical formula, but the zirconolite has many impurities in its composition. The Nb concentration can reach 0.6 apfu. and the Fe content reaches 0.5 apfu.,

which is close to the chemical composition of laachite [37]. Such chemical compositions for zirconolite are more typical of volcanic regions [38,39]; however, there are references to minerals similar in composition to laachite in carbonatites, for example, in the Chuktukon complex [58]. The chemical composition of pyrochlore in FOS 1 is relatively enriched in Ti and Ta is practically absent, and thus can be called Ti-pyrochlores according to a special nomenclature proposed by Yaroshevskii and Bagdasarov [59]. Such compositions are typical of carbonatites and associated phoscorites. Pyrochlores without tantalum have been described for carbonatites that crystallized during the final stages of evolution [60]. In the pyrochlores of FOS 1, low concentrations of REE are also noted, usually ranging from 0.05 to 0.14 f.u in total. REEs are widespread in pyrochlores of carbonatite deposits: for example, in the carbonatites of Siberia [61] and the Lovozero massif [62]. According to Yaroshevskii and Bagdasarov [59], no visible correlation of REE with Na or Ti has been observed in pyrochlores, while in FOS 1 pyrochlores, the detectable depletion of Ca occurs due to isomorphic substitution according to the Ca + Nb ⇔ REE + Ti scheme.

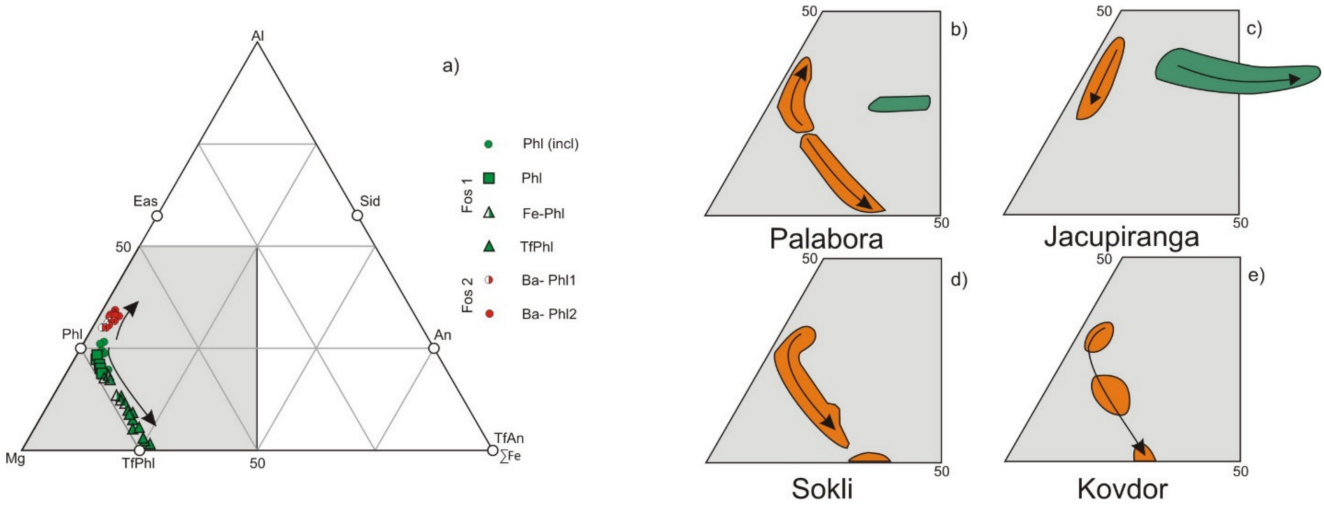


Figure 12. Trends of changes in mica of the Arbarastakh phoscorites (**a**) and other carbonatite complexes (**b**–**e**). Palabora [13], Jacupiranga [28], Sokli [51], Kovdor [34]. Green field—micas of accompanying silicate rocks, orange field—micas of carbonatites and phoscorites. Phl—phlogopite, TfPhl—teraferriphlogopite, TfAn—tetraferriannite, An—annite, Sid—siderophyllite, Eas—eastonite (data by [25], supplemented by the authors). Due to the absence of Ba in the graphs, the differentiation of phlogopites in the phlogopite—kinoshitalite and phlogopite—eastonite series is impossible in these graphs but is explained in the text.

For FOS 2, the main accessory mineral is pyrochlore of two varieties: Ta-pyrochlore (inclusions in magnetite) and Th-pyrochlore (zonal grains). All of these pyrochlores are enriched in Ta. The tantalum concentration in Th-pyrochlore generally does not exceed 0.15 apfu. and has analogues in carbonatites of the early stage, and for Ta-pyrochlore, the value can reach 0.7 apfu., which is not typical for carbonatites. Such mineral phases have also been found in the albitized carbonatites of the Srednaya Zima [63].

The minerals of the pyrochlore group generally contain Th, but high concentrations (>0.2 apfu.) are extremely rare [40,64–66]. In the literature, Th-pyrochlore is described as the most recent (relative to other pyrochlores of the massif) and occurs mainly in phoscorites (for example, the Vuorjärvi massif) or "oceanic" carbonatites (e.g., Cape Verde Archipelago) [59]. In FOS 2 zonal pyrochlores, the Th concentration reaches 0.4 apfu., and a small concentration of U (0.05–0.2 apfu.) is also noted. Despite these elements occurring together, their content has a negative correlation (Figure 10b). This correlation has been described earlier [59], and the authors noted that Th and U are often "antagonists". Due to the enrichment of Arbarastakh pyrochlores with these elements, a characteristic depletion of Na is observed in relation to the empirical formula, but there is no deficiency of cations

in the A position. On the contrary, there is more often an overabundance in this position, which leads to an increase in charge. In addition, Th-pyrochlore is characterized by Zr impurity up to 0.15 apfu. (Figure 9). Such concentrations are generally found in pyrochlores of carbonatites [36,67,68] and are considered to limit the B position. The outermost parts of the grains are often enriched in Ba, Ti, and, to a lesser extent, REE. This enrichment is likely associated with post-magmatic processes; when the partial dissolution of the phlogopite saturated with these elements occurred, subsequent enrichment of the pyrochlore took place, and, finally, the crystallization of barite.

6. Conclusions

Thus, having summarized the data on the evolution of the chemical composition of the minerals in FOS 1 and FOS 2, the sequence of crystallization of phoscorites remains unclear. A large amount of olivine in FOS 1 should indicate that phoscorites FOS 1 formed earlier than FOS 2. However, the chemical composition of the FOS 2 magnetite should be "purified" of impurities (Ti, Mg, Al) if differentiation occurred, but instead, an increase in Al and Mg is observed in FOS 2. In FOS 2 phlogopite, the Al concentration should decrease, and Fe should increase; however, the inverse relationship is observed. In addition, for all the minerals in phoscorites, linear dependences of chemical compositions are observed for individual minerals directly within a group of phoscorites. Simultaneously, the chemical compositions of individual minerals do not have a consistent linear change for all phoscorites, and they form discrete groups. This allows us to assume that the studied phoscorites were formed by the sequential introduction of various portions of the melt. FOS 1 in relation to FOS 2 was enriched in Zr (accommodated in baddeleyite and zirconolite) and REE (accommodated in apatite, zirconolite, pyrochlore); FOS 2, in turn, was enriched in Al (magnetite and phlogopite), Ba (phlogopite, pyrochlore rims, barite), Nb, Ta (Ta-pyrochlore), Th, U (Th-pyrochlore) and, to a lesser extent, Sr (Th-pyrochlore, strontianite).

According to the study of melt inclusions in FOS 1, Prokopiev and other [25] assumed that phoscorites are a product of silicocarbonatite melt differentiation. In this regard, we plan to further study the chemical composition of minerals of silicocarbonatite and carbonatite minerals of the Arbarastakh complex.

Supplementary Materials: The following are available online at https://www.mdpi.com/article/10.3390/min11060556/s1, Electronic Supplement 1: The Analytical Conditions and the Set of Standards. Table S1. The spreadsheets with microprobre results and apfu calculation.

Author Contributions: Conceptualization, M.N.K. and A.G.D.; data curation, M.N.K. and A.G.D.; investigation, M.N.K., I.R.P. and I.A.I.; methodology, M.N.K. and A.G.D.; project administration, A.G.D.; writing—original draft, M.N.K. and A.G.D.; writing—review and editing, M.N.K. and A.G.D. All authors have read and agreed to the published version of the manuscript.

Funding: The investigations were supported by the Russian Science Foundation (RSF), project #19-17-00019.

Data Availability Statement: Not Applicable.

Acknowledgments: Analytical equipment for this study was provided by the Analytical Center for multi-elemental and isotope research SB RAS, Novosibirsk, Russia. The work was done on state assignment of IGM SB RAS (0330-2016-0002) and GIN SB RAS (AAAA-A21-121011390002-2).

Conflicts of Interest: The authors declare no conflict of interest.

References

1. Wallace, M.E.; Green, D.H. An experimental determination of primary carbonatite magma composition. *Nature* **1988**, *335*, 343–346. [CrossRef]
2. Dalton, J.A.; Wood, B.J. The compositions of primary carbonate melts and their evolution through wall rock reaction in the mantle. Earth and Planet. *Sci. Lett.* **1993**, *119*, 511–525.
3. Harmer, R.E.; Gittins, J. The Case for Primary, Mantle-derived Carbonatite Magma. *J. Petrol.* **1998**, *39*, 1895–1903. [CrossRef]

4. Otto, J.W.; Wyllie, P.J. Relationships between silicate melts and carbonate-precipitating melts in CaO–MgO–SiO_2–CO_2–H_2O at 2 kbar. *Mineral. Petrol.* **1993**, *48*, 343–365.
5. Kjarsgaard, B.; Hamilton, D.L. Carbonatite origin and diversity. *Nature* **1989**, *338*, 547–548. [CrossRef]
6. Lee, W.; Wyllie, P.J. Petrogenesis of carbonatite magmas from mantle to crust, constrained by the system CaO-(MgO-FeO)-(Na_2O-K_2O)-(SiO_2-Al2O_3-TiO_2)-CO_2. *J. Petrol.* **1998**, *39*, 495–517. [CrossRef]
7. Wall, F.; Zaitsev, A.N. *Phoscorites and Carbonatites from Mantle to Mine: The Key Example of the Kola Alkaline Province*; Mineralogical Society: London, UK, 2004; p. 498, Series 10.
8. Chakhmouradian, A.R. High-field-strength elements in carbonatitic rocks: Geochemistry, crystal chemistry and significance for constraining the sources of carbonatites. *Chem. Geol.* **2006**, *235*, 138–160. [CrossRef]
9. Chakhmouradian, A.R.; Wall, F. Rare earth elements: Minerals, mines, magnets (and more). *Elements* **2012**, *8*, 333–340. [CrossRef]
10. Wall, F. *Rare Earth Elements. Critical Metals Handbook*; John Wiley & Sons: Hoboken, NJ, USA, 2013. [CrossRef]
11. Smith, M.P.; Campbell, L.S.; Kynicky, J. A review of the genesis of the world-class Bayan Obo Fe-REE-Nb deposits, Inner Mongolia, China: Multistage processes and outstanding questions. *Ore Geol. Rev.* **2014**, *64*, 459–476. [CrossRef]
12. Chakhmouradian, A.R.; Reguir, E.P.; Kressall, R.D.; Crozier, J.; Pisiak, L.K.; Sidhu, R.; Yang, P. Carbonatite-hosted niobium deposit at Aley, northern British Columbia (Canada): Mineralogy, geochemistry and petrogenesis. *Ore Geol. Rev.* **2015**, *64*, 642–666. [CrossRef]
13. Giebel, R.J.; Marks, M.A.W.; Gauert, C.D.K.; Markl, G. A model for the formation of carbonatite–phoscorite assemblages based on the compositional variations of mica and apatite from the Palabora Carbonatite Complex, South Africa. *Lithos* **2019**, *324*, 89–104. [CrossRef]
14. Barbosa, E.S.R.; Brod, J.A.; Cordeiro, P.F.O.; Junqueira-Brod, T.C.; Santos, R.V.; Dantas, E.L. Phoscorites of the Salitre I complex: Origin and petrogenetic implications. *Chem. Geol.* **2020**, *535*, 119463. [CrossRef]
15. Krasnova, N.; Petrov, T.; Balaganskaya, E.; Garcia, D.; Moutte, J.; Zaitsev, A.; Wall, F. Introduction to phoscorites: Occurrence, composition, nomenclature and petrogenesis. In *Phoscorites and Carbonatites from Mantle to Mine: The Key Example of the Kola Alkaline Province*; Wall, F., Zaitev, A.N., Eds.; The Mineralogical Society of Great Britain and Ireland: London, UK, 2004; pp. 45–74.
16. Kukharenko, A.A.; Orlova, M.P.; Bulakh, A.G.; Bagdasarov, E.A.; Rimskaya-Korsakova, O.M.; Nefedov, E.I.; Ilinskiy, G.A.; Sergeev, A.S.; Abakumova, N.B. The Caledonian Complex of Ultramafic, Alkaline Rocks and Carbonatites of the Kola Peninsula and Northern Karelia. Nedra: Saint Petersburg, Russia, 1965; p. 772. (In Russian)
17. von Backstrom, J.W.; Jacob, R. E Uranium in South Africa and South West Africa (Namibia). *Philos. Trans. R. Soc. Lond.* **1979**, *291*, 307–319.
18. Lapin, A.V.; Vartiainen, H. Orbicular and spherulitic carbonatites from Sokli and Vuorijarvi. *Lithos* **1983**, *16*, 53–60. [CrossRef]
19. Klemme, S. Experimental constrains on the evolution of iron and phosphorus-rich melts: Experiments in the system CaO–MgO–Fe_2O_3–P_2O_5–SiO_2–H_2O–CO_2. *J. Mineral. Petrol. Sci.* **2010**, *105*, 1–8. [CrossRef]
20. Bell, K.; Kjarsgaard, B.A.; Simonetti, A. Carbonatites into the twenty–first century. *J. Petrol.* **1998**, *39*, 1839–1845. [CrossRef]
21. Belov, S.V.; Lapin, A.V.; Tolstov, A.V.; Frolov, A.A. Metallogeny of Platform Magmatism (Traps, Carbonatites, Kimberlites). SO RAN: Novosibirsk, Russia, 2008; p. 537. (In Russian)
22. Veksler, I.V.; Dorfman, A.M.; Dulski, P.; Kamenetsky, V.S.; Danyushevsky, L.V.; Jeffries, T.; Dingwell, D.B. Partitioning of elements between silicate melt and immiscible fluoride, chloride, carbonate, phosphate and sulfate melts, with implications to the origin of natrocarbonatite. *Geochim. Cosmochim. Acta* **2012**, *79*, 20–40. [CrossRef]
23. Glagolev, A.A.; Korchagin, A.M.; Kharchenkov, A.G. *Arbarastakh and Inagli Alkaline-Ultrabasic Massifs*; Nauka: Moscow, Russia, 1974; p. 175. (In Russian)
24. Yarmolyuk, V.V.; Kovalenko, V.I.; Sal'nikova, E.B.; Nikiforov, A.V.; Kotov, A.B.; Vladykin, N.V. Late Riphean rifting and breakup of Laurasia: Data on geochronological studies of ultramafic alkaline complexes in the southern framing of the Siberian craton. *Dokl. Earth Sci.* **2005**, *404*, 1031–1037.
25. Prokopyev, I.R.; Doroshkevich, A.G.; Zhumadilova, D.V.; Starikova, A.E.; Nugumanova Ya, N.; Vladykin, N.V. Petrogenesis of Zr–Nb (REE) carbonatites and phoscorites from the Arbarastakh complex (Aldan Shield, Russia): Mineralogy and inclusion data. *Ore Geol. Rev.* **2021**, *131*, 104042. [CrossRef]
26. Smelov, A.P.; Zedgenizov, A.N.; Timofeev, V.F. *Aldan-Stanovoy Shield//Tectonics, Geodynamics and Metallogeny of the Territory of the Republic of Sakha (Yakutia)*; MAIK Science/Interperiodica: Moscow, Russia, 2001; pp. 81–104. (In Russian)
27. Rieder, M.; Cavazzini, G.; D'Yakonov, Y.; Frank-Kamenetskii, V.A.; Guggenheim, S.; Koval, P.V.; Muller, G.; Neiva, A.M.R.; Radoslovich, E.W.; Robert, J.-L.; et al. Nomenclature of micas. *Can. Mineral.* **1998**, *36*, 905–912. [CrossRef]
28. Brod, J.; Gaspar, J.; De Araújo, D.; Gibson, S.; Thompson, R.; Junqueira-Brod, T. Phlogopite and tetra-ferriphlogopite from Brazilian carbonatite complexes: Petrogenetic constraints and implications for mineral-chemistry systematics. *J. Asian Earth Sci.* **2001**, *19*, 265–296. [CrossRef]
29. Atencio, D.; Andrade, M.; Christy, A.G.; Giere, R. The pyrochlore Supergroup of Minerals: Nomenclature. *Can. Mineral.* **2010**, *48*, 569–594. [CrossRef]
30. Hogarth, D. Pyrochlore, apatite and amphibole: Distinctive minerals in carbonatite. In *Carbonatites: Genesis and Evolution*; Bell, K., Ed.; Unwin Hyman: London, UK, 1989; pp. 105–148.
31. Klemme, S.; Dalpé, C. Trace-element partitioning between apatite and carbonatite melt. *Am. Miner.* **2003**, *88*, 639–646. [CrossRef]

32. Teiber, H.; Marks, M.A.; Arzamastsev, A.A.; Wenzel, T.; Markl, G. Compositional variation in apatite from various host rocks: Clues with regards to source composition and crystallization conditions. *Neues Jahrb. Für Mineral. Abh.* **2015**, *192*, 151–167. [CrossRef]
33. Chakhmouradian, A.R.; Reguir, E.P.; Zaitsev, A.N.; Couëslan, C.; Xu, C.; Kynický, J.; Mumin, A.H.; Yang, P. Apatite in carbonatitic rocks: Compositional variation, zoning, element partitioning and petrogenetic significance. *Lithos* **2017**, *274*, 188–213. [CrossRef]
34. Krasnova, N.; Balaganskaya, E.; Garcia, D. Kovdor—classic phoscorites and carbonatites. In *Phoscorites and Carbonatites from Mantle to Mine: The Key Example of the Kola Alkaline Province*; Wall, F., Zaitev, A.N., Eds.; Mineralogical Society of Great Britain and Ireland: London, UK, 2004; pp. 99–132.
35. Fleet, M.E. Sheet silicates: Micas. In *Rock-Forming Minerals*; Deer, W.A., Howie, R.A., Zussman, J., Eds.; Geological Society of London: London, UK, 2003; p. 765.
36. Williams, C.T.; Gieré, R. Zirconolite: A Review of Localities Worldwide, and a Compilation of its Chemical Compositions. *Bull Nat. Hist. Mus. Lond.* 1996, 52, pp. 1–24. Available online: http://repository.upenn.edu/ees_papers/95 (accessed on 20 May 2021).
37. Chukanov, N.V.; Krivovichev, S.V.; Pakhomova, A.S.; Pekov, I.V.; Schafer, C.; Vigasina, M.F.; Van, K.V. Laachite, (Ca,Mn)2Zr2Nb2TiFeO14, a new zirconolite-related mineral from the Eifel volcanic region, Germany. *Eur. J. Miner.* **2014**, *26*, 103–111. [CrossRef]
38. Zubkova, N.V.; Chukanov, N.V.; Pekov, I.V.; Ternes, B.; Schuller, W.; Ksenofontov, D.A.; Pushcharovsky, D.Y. The crystal structure of nonmetamict Nb-Rich zirconolite–*3T* from the Eifel paleovolcanic region, Germany. *Zeitschrift Kristallographie* **2018**, *233*, 463–468. [CrossRef]
39. Chukanov, N.V.; Zubkova, N.V.; Britvin, S.N.; Pekov, I.V.; Vigasina, M.F.; Schafer, C.; Ternes, B.; Schuller, W.; Polekhovsky, Y.S.; Ermolaeva, V.N.; et al. Nöggerathite-(Ce),(Ce,Ca)2Zr2(Nb,Ti)(Ti,Nb)2Fe2+O14,a New Zirconolite-Related Mineral from the Eifel Volcanic Region, Germany. *Minerals* **2018**, *8*, 449. [CrossRef]
40. Kogarko, L.N.; Sorokhtina, N.V.; Zaitsev, V.A.; Senin, V.G. Rare Metal Mineralization of Calcite Carbonatites from the Cape Verde Archipelago. *Geochem. Int.* **2008**, *47*, 531–549.
41. Zaitsev, A.N.; Williams, C.T.; Wall, F.; Zolotarev, A. Evolution of Chemical Composition of Pyrochlore Group Minerals from Phoscorites and Carbonatites of the Khibina Alkaline Massif. *Geol. Ore Depos.* **2012**, *7*, 503–515. [CrossRef]
42. Hogarth, D.D. Classification and nomenclature of the pyrochlore group. *Am. Mineral.* **1977**, *62*, 403–410.
43. Lee, M.J.; Garcia, D.; Moutte, J.; Williams, C.T.; Wall, F. Carbonatites and phoscorites from the Sokli Complex, Finland. In *Phoscorites and Carbonatites from Mantle to Mine*; Mineralogical Society of Great Britain and Ireland: London, UK, 2004; Volume 5, pp. 133–162. [CrossRef]
44. McCormick, G.R.; Le Bas, M.J. Phlogopite crystallization in carbonatitic magmas from Uganda. *Can. Mineral.* **1996**, *34*, 469–478.
45. Edgar, A.D.; Arima, M. Fluorine and chlorine contents of phlogopites crystallized from ultrapotassic rock compositions in high pressure experiments; implication for halogen reservoirs in source regions. *Am. Mineral.* **1985**, *70*, 529–536.
46. Edgar, A.D.; Arima, M. Conditions of phlogopite crystallization in ultrapotassic volcanic rocks. *Min. Mag.* **1983**, *47*, 11–19. [CrossRef]
47. Tronnes, R.; Edgar, A.; Arima, M. A high pressure-high temperature study of TiO2 solubility in Mg-rich phlogopite: Implications to phlogopite chemistry. *Geochim. Cosmochim. Acta* **1985**, *49*, 2323–2329. [CrossRef]
48. Kogarko, L.; Ryabchikov, I.; Kuzmin, D. High-Ba mica in olivinites of the Guli massif (Maimecha–Kotui province, Siberia). *Russ. Geol. Geophys.* **2012**, *53*, 1209–1215. [CrossRef]
49. Clarke, L.; Le Bas, M.; Spiro, B. Rare Earth, Trace Element and Stable Isotope Fractionation of Carbonatites at Kruidfontein, Transvaal, South Africa. In Proceedings of the 5th International Kimberlite Conference: Extended Abstracts, Araxá, Brazil; 1991; pp. 49–51.
50. Heathcote, R.C.; McCormick, G.R. Major-cation substitution in phlogopite and evolution of carbonatite in the Potash Sulphur Springs complex, Garland County, Arkansas. *Am. Mineral.* **1989**, *74*, 132–140.
51. Lee, M.J.; Garcia, D.; Moutte, J.; Lee, J.I. Phlogopite and tetraferriphlogopite from phoscorite and carbonatite associations in the Sokli massif, Northern Finland. *Geosci. J.* **2003**, *7*, 9–20. [CrossRef]
52. Veksler, I.V.; Keppler, H. Partitioning of Mg, Ca, and Na between carbonatite melt and hydrous fluid at 0.1–0.2 GPa. *Contrib. Min. Pet.* **2000**, *138*, 27–34. [CrossRef]
53. Doroshkevich, A.; Veksler, I.; Izbrodin, I.; Ripp, G.; Khromova, E.; Posokhov, V.; Travin, A.; Vladykin, N. Stable isotope composition of minerals in the Belaya Zima plutonic complex, Russia: Implications for the sources of the parental magma and metasomatizing fluids. *J. Asian Earth Sci.* **2016**, *116*, 81–96. [CrossRef]
54. Giebel, R.J.; Gauert, C.D.; Marks, M.A.W.; Costin, G.; Markl, G. Multi-stage formation of REE minerals in the Palabora Carbonatite Complex, South Africa. *Am. Min.* **2017**, *102*, 1218–1233. [CrossRef]
55. Rimskaya-Korsakova, O.M.; Krasnova, N.I.; Kopulova, L.N. Typical chemical features of apatites of the Kovdor complex deposit. *Mineral. Geochem.* **1979**, *6*, 58–70. (In Russian)
56. Brassinnes, S.; Balaganskaya, E.; Demaiffe, D. Magmatic evolution of the differentiated ultramafic, alkaline and carbonatite intrusion of Vuoriyarvi (Kola Peninsula, Russia). A LA-ICP-MS study of apatite. *Lithos* **2005**, *85*, 76–92. [CrossRef]
57. Mangler, M.F.; Marks, M.A.W.; Zaitzev, A.N.; Eby, G.N.; Markl, G. Halogen (F,Cl, and Br) at Oldoinyo Lengai volcano (Tanzania): Effects of magmatic differentiation, silicate–natrocarbonatite melt separation and surface alteration of natrocarbonatite. *Chem. Geol.* **2014**, *365*, 43–53. [CrossRef]

58. Chebotarev, D.A.; Doroshkevich, A.G.; Klemd, R.; Karmanov, N.S. Evolution of Nb-mineralization in the Chuktukon carbonatite massif, Chadobets upland (Krasnoyarsk Territory, Russia). *Period. Di Mineral.* **2017**, *86*, 99–118.
59. Yaroshevsky, A.; Bagdasarov, Y.A. Geochemical Variety of Pyrochlore-Group Minerals. *Geokhimiya* **2008**, *46*, 1245–1266.
60. Groulier, P.A.; Turlin, F.; André-Mayer, A.S.; Ohnenstetter, D.; Crépon, A. Silicate-carbonate liquid immiscibility: Insights from the Crevier alkaline intrusion (Quebec). *J. Petrol.* **2020**, *61*, egaa033. [CrossRef]
61. Lapin, A.V.; Kulikova, I.M. Alteration processes in pyrochlore and their products in weathering crusts of carbonatites. *Zap. Vsesoyuznogo Mineral. Obs.* **1989**, *118*, 41–49. (In Russian)
62. Pekov, I.V. Genetic Mineralogy and Crystal Chemistry of Trace Elements in Highly Alkaline Postmagmatic Systems. Doctoral Dissertation, Moscow State University, Moscow, Russia, 2005.
63. Bagdasarov, Y.A. On the Distribution of Rare-Metal Mineralization in Carbonatites. *Zap. Vses. Miner. Ova.* **1969**, *98*, 395–406.
64. Gaidukova, V.S.; Zdorik, T.B. Trace-Element Minerals in Carbonatites. In *Geology of Trace-Element Deposits. Issue 17. Geological Structure and Mineralogical–Geochemical Features of Rare-Metal Carbonatites*; Gosgeoltekhizdat: Moscow, Russia, 1962; pp. 86–117. (In Russian)
65. Williams, T.; Kogarko, L.N. New Data on Rare-Metal Mineralization in the Guli Massif Carbonatites, Arctic Siberia. *Geochem. Int.* **1996**, *34*, 433–440.
66. Subbotin, V.V.; Subbotina, G.F. Pyrochlore Group Minerals in the Phoscorites and Carbonatites of the Kola Peninsula Vestn. *Murm. Gos. Tekhn. Univ.* **2000**, *3*, 273–284.
67. Perrault, G. La composition chimique et la structure crystalline du pyrochlore d'Oka, P.Q. *Can. Mineral.* **1968**, *9*, 383–402.
68. Epshtein, E.M.; Danil'chenko, N.A.; Nechelyustov, G.N. Hypogenic Bariopyrochlore from a Carbonatite Complex. *Zap. Vseross. Mineral.* **1991**, *120*, 74–79.